

Model Development and Analysis of the Fate and Transport of Water in a Salt- Based Repository

Fuel Cycle Research & Development

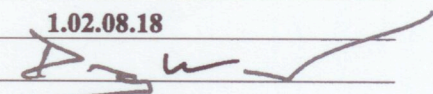
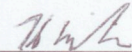
Prepared for
U.S. Department of Energy
Used Fuel disposition
**Philip Stauffer, Dylan Harp, Bruce A.
Robinson, LANL**
September 28, 2012
Milestone M2FT-12LA08180112
LANL Report LA-UR-12-25050
FCRD-UFD-2012-000386



DISCLAIMER

This information was prepared as an account of work sponsored by an agency of the U.S. Government. Neither the U.S. Government nor any agency thereof, nor any of their employees, makes any warranty, expressed or implied, or assumes any legal liability or responsibility for the accuracy, completeness, or usefulness, of any information, apparatus, product, or process disclosed, or represents that its use would not infringe privately owned rights. References herein to any specific commercial product, process, or service by trade name, trade mark, manufacturer, or otherwise, does not necessarily constitute or imply its endorsement, recommendation, or favoring by the U.S. Government or any agency thereof. The views and opinions of authors expressed herein do not necessarily state or reflect those of the U.S. Government or any agency thereof.

Appendix E FCT Document Cover Sheet

Name/Title of Deliverable/Milestone	Report on Model Development and Analysis of the Fate and Transport of Water in Salt-Based Repository / M2FT-12LA08180112
Work Package Title and Number	Salt Disposal Initiative-LANL / FT12LA081801
Work Package WBS Number	1.02.08.18
Responsible Work Package Manager	Doug Weaver /  (Name/Signature)
Date Submitted <u>9/28/12</u>	
Quality Rigor Level for Deliverable/Milestone	<input checked="" type="checkbox"/> -QRL-3 <input type="checkbox"/> QRL-2 <input type="checkbox"/> QRL-1 <input type="checkbox"/> N/A* <input type="checkbox"/> Nuclear Data
This deliverable was prepared in accordance with	<u>Los Alamos National Laboratory</u> (Participant/National Laboratory Name)
QA program which meets the requirements of	
<input checked="" type="checkbox"/> DOE Order 414.1 <input type="checkbox"/> NQA-1-2000 <input type="checkbox"/> Other	
This Deliverable was subjected to:	
X Technical Review Technical Review (TR) Review Documentation Provided <input type="checkbox"/> Signed TR Report or, <input type="checkbox"/> Signed TR Concurrence Sheet or, X Signature of TR Reviewer(s) below Name and Signature of Reviewers <u>Hari S. Viswanathan / </u>	<input type="checkbox"/> Peer Review Peer Review (PR) Review Documentation Provided <input type="checkbox"/> Signed PR Report or, <input type="checkbox"/> Signed PR Concurrence Sheet or, <input type="checkbox"/> Signature of PR Reviewer(s) below

**NOTE In some cases there may be a milestone where an item is being fabricated, maintenance is being performed on a facility, or a document is being issued through a formal document control process where it specifically calls out a formal review of the document. In these cases, documentation (e.g., inspection report, maintenance request, work planning package documentation or the documented review of the issued document through the document control process) of the completion of the activity along with the Document Cover Sheet is sufficient to demonstrate achieving the milestone. QRL for such milestones may also be marked N/A in the work package provided the work package clearly specifies the requirement to use the Document Cover Sheet and provide supporting documentation.*

LA-UR-12-25050

Approved for public release; distribution is unlimited.

Title: Report on Model Development and Analysis of the Fate and Transport of Water in a Salt-Based Repository

Author(s): Stauffer, Philip H.
Harp, Dylan R.
Robinson, Bruce A.

Intended for: Report



Disclaimer:

Los Alamos National Laboratory, an affirmative action/equal opportunity employer, is operated by the Los Alamos National Security, LLC for the National Nuclear Security Administration of the U.S. Department of Energy under contract DE-AC52-06NA25396. By approving this article, the publisher recognizes that the U.S. Government retains nonexclusive, royalty-free license to publish or reproduce the published form of this contribution, or to allow others to do so, for U.S. Government purposes. Los Alamos National Laboratory requests that the publisher identify this article as work performed under the auspices of the U.S. Department of Energy. Los Alamos National Laboratory strongly supports academic freedom and a researcher's right to publish; as an institution, however, the Laboratory does not endorse the viewpoint of a publication or guarantee its technical correctness.

LANL Milestone M2FT-12LA08180112

Report on:
Model Development and Analysis
of the Fate and Transport of Water
in a Salt-Based Repository

September 28, 2012

Philip Stauffer
Dylan Harp
Bruce A. Robinson

I. Executive Summary

In March, 2012, a workshop was convened that included the Department of Energy Office of Nuclear Energy (DOE-NE) and Office of Environmental Management (DOE-EM), as well as Los Alamos National Laboratory (LANL) and Sandia National Laboratories (SNL) to develop plan for a generic salt research effort. The outcome for this workshop was a plan for an 18-month study designed to conduct initial research and to establish the future direction for salt R&D initiatives in the U.S.. A series of data compilation, laboratory experiments, and modeling activities were initiated, including the development of coupled thermal-mechanical- hydrologic -chemical (TMHC) models that could be used to predict the evolution of a repository after waste emplacement. The approach called for in the TMHC activity is to leverage existing computational models and tools to couple TM, TH, and C phenomena in salt under subsurface repository conditions, with a particular focus on brine accessibility and moisture transport.

To this end, the present study summarizes the initial work of LANL on numerical modeling related to nuclear waste storage in a salt repository. The principle goal of the work is to benchmark the LANL developed porous flow simulator, FEHM, to the results of experiments performed at the Waste Isolation Pilot Plant (WIPP) under the restricted conditions in which the system can be modeled assuming thermal and hydrologic processes dominate the behavior. As such, the work is a preliminary effort at simulating the fluid flow and heat transport processes, before treating the fully coupled thermal-mechanical-hydrologic-chemical (TMHC) coupled processes in the future.

The experiments chosen for the benchmarking exercise were originally performed to gather data and insight into how high level nuclear waste will impact salt in a repository setting. These experiments involved drilling boreholes into the floors of WIPP rooms and emplacing heaters in the holes. During the experiments, water flow from the surrounding salt into the boreholes was measured.

The benchmarking presented in this report explores the ability of the numerical simulations to accurately capture several aspects of the experiments. The report begins with a section wherein FEHM is used to recreate analytical model results associated with the experimental effort. This step is crucial to give confidence that FEHM is working for the types of simulations needed to correctly model the migration of brine in a salt repository. Next, FEHM is used to simulate the experimental boreholes during the period before heating occurs. Then, simulations are performed to explore the impacts of increased temperature on the system.

The final sections of the report describe initial creation of a three-dimensional drift scale heater simulation in a hypothetical salt repository. These proof of concept simulations show the direction that LANL will take in moving from the benchmark heater scale simulations to larger repository scale simulations. Some of these simulations are performed with no water flow to provide a baseline for discussion of likely processes when water and water vapor are included. Then, a preliminary thermal-hydrologic model is presented to make an initial assessment of the redistribution of water within the drift and surrounding salt, and to determine the extent to which the presence of water affects the thermal regime and temperature distribution. If a field heater test is conducted, these results will inform the design of measurement systems that maximize the scientific value of the field campaign. The report concludes with a discussion of the path forward for making additional progress in addressing outstanding modeling issues.

II. Background on the WIPP Experiments

The benchmarking presented in this report explores the ability of the numerical simulations to accurately recreate results originally obtained at the WIPP site in the mid 1980s. The experiments we consider were performed starting in April 1985. The experimental results and subsequent analysis through analytical modeling are summarized in a 1988 Sandia report entitled “Brine Inflow to WIPP Disposal Rooms: Data, Modeling, and Assessment” (Nowak et al., 1988).

The experiments were performed to gain understanding of the mechanisms associated with water migration into a void created by drilling in bedded salt at WIPP and the impacts of heat on water release; the studies also provide a basis for quantification of these processes.

Boreholes in the range of 30-36 inch diameter were drilled into the floors of two WIPP rooms and used for the brine inflow experiments. Additional experiments looked at non-heated flow into small (~3 inch) diameter boreholes. Results from the WIPP experiments suggest that before heating, inflow rates of 5-15 g/day are typical, whereas after heating brine inflow rates increased to maximum before decreasing (Figure II.1). When a hole is drilled, either a borehole or an underground drift, the atmospheric pressure in the hole creates a pressure driving force from the far field (which is a pressure somewhere between the hydrostatic and lithostatic pressures at that location) toward the hole. The far field pressure is generally not known, and in several benchmarking models presented later, different values within the range from hydrostatic and lithostatic are used to enable comparison to previous results.

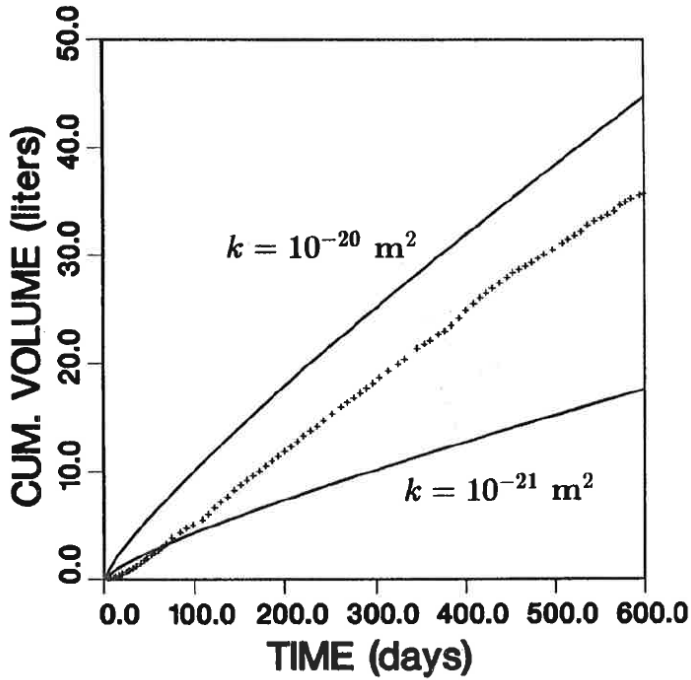


Figure II.1 Brine production data (plus signs) from Nowak et al., 1988, compared to simple analytical model results of fluid migration in the absence of heating. The salt permeability k in the region around the borehole is the parameter that controls the flux into the borehole.

III. Brief introduction to FEHM

The Finite Element Heat and Mass Transfer Code, FEHM, has been developed by LANL for more than 30 years (Zyvoloski, 2007). The code started as a tool to simulate the hot-dry rock experiments, but has grown over the years to include unsaturated flow, reactive chemistry, stress, and carbon dioxide (fehm.lanl.gov). FEHM has been used in more than 100 peer reviewed publications (FEHM 2012). FEHM uses a finite volume method for solving multiphase flow and transport, while using a finite element formulation for the fully coupled stress solutions. Capabilities pertinent to the salt simulations presented in this report include the ability to run fully coupled heat and mass transfer on both 2-D radial and 3-D numerical meshes. Simulations presented herein make use of a simplified pressure/porosity relationship that allows us to begin work on the impacts of changing pore pressure on flow. However the fully coupled stress/flow solution will permit more sophisticated simulations as the project evolves. Additionally, the reactive chemistry components of the code will also be quite useful because project plans call for the study of water source terms associated with pressure within fluid inclusions that can result in fluid migration to grain boundaries, and intergranular flow toward the low-pressure opening. The reactive chemistry section of the code will also allow us to explore clay hydration/dehydration reactions and their impacts on repository performance.

In this initial work, we ignore the large-scale deformation processes due to salt creep that will dramatically impact the sealing of the repository in the long run. Therefore, our results are relevant to the initial evolution of the thermal regime and water transport processes during the initial heat-up of the repository. A firm understanding of these processes is required to enable better prediction of the long-term behavior of the system. For example, if the presence of water has an impact on salt fracture healing and crushed salt consolidation, then characterization of the water balance in the drift and surrounding salt will be required.

In addition to standard heat-mass-stress, FEHM has been modified to include two models for salt thermal conductivity as a function of temperature (Clayton and Gable, 2009). This is important as the thermal conductivity of intact salt decreases by nearly 30% from 30 °C to 130 °C. First, intact salt follows the Munson et al. (1990) relationship:

$$\lambda_{salt}(T) = \lambda_{300} \left(\frac{300}{T} \right)^Y$$

where λ_{300} is the thermal conductivity of salt at $T = 300$ K (5.4 W/m-K), and γ is a material constant of 1.14. The thermal conductivity of crushed salt is based on the BAMBUS II study (Bechtold et al., 2004) and results in the following equation (From Clayton and Gable, 2009):

$$\lambda_{c-salt}(T) = k_{cs}(\varphi) \left(\frac{300}{T} \right)^\gamma$$

With the porosity (φ) dependent thermal conductivity k_{cs} as:

$$k_{cs}(\varphi) = (-270\varphi^4 + 370\varphi^3 - 136\varphi^2 + 1.5\varphi + 5) \cdot 1.08$$

IV. Benchmarking FEHM against analytical models based on past studies

a. Isothermal Analytical

Deal and Case (1987) present graphical results for the total flux into 20 experimental boreholes excavated at the Waste Isolation Pilot Plant (WIPP). Nowak et al. (1988) assess the salt permeability at WIPP based on these data using an analytical model of transient Darcy flow in a porous medium. The basis of the model is the isothermal diffusion equation, defined as

$$\frac{\partial p}{\partial t} = c \nabla^2 p,$$

where p is the fluid pore pressure, c is the fluid diffusivity, and t is time. The fluid diffusivity c depends on permeability, fluid viscosity, and the elastic properties of the fluid and solid. The excavated borehole at depth is idealized in the model using an initial condition of constant pore pressure as

$$p(r, t = 0) = p_0,$$

where r is the radius from the center of the borehole and p_0 is the initial pressure. Boundary conditions set the pressure at zero at the borehole walls and p_0 at the far field as

$$p(a, t) = 0$$

and

$$\lim_{r \rightarrow \infty} p(r, t) = p_0,$$

$$\lim_{r \rightarrow \infty} p(r, t) = p_0,$$

where a is the borehole radius. Solving these equations for flux at the borehole wall (Crank, 1979) produces

$$q(a, t_*) = \frac{4kp_0}{\pi^2 \mu a} \int_0^\infty \frac{\exp(-u^2 t_*)}{J_0^2(u) + Y_0^2(u)} \frac{du}{u}$$

where k is permeability, μ is fluid viscosity, $t_* = ct/a^2$ is dimensionless time, and $J_0(x)$ and $Y_0(x)$ are zero-order Bessel functions of the first and second kind, respectively. Nowak et

al. (1988) estimated permeabilities using this result and the data from Deal and Case (1987).

Assumptions in the analytical model include (1) the porous medium is saturated (Darcy flow), (2) a limitless interconnected network of pores exist extending out to the far field, (3) and the brine flow is radially symmetric.

i. FEHM representation of the isothermal analytical model

Numerical models were developed to simulate isothermal flow into the boreholes discussed in Deal and Case (1987) using FEHM. The boreholes are idealized in the numerical model as a 2D radial slice of a borehole 0.01 m thick. The actual length of boreholes are accounted for by multiplying the simulation results by the actual borehole length in centimeters (the simulation is a borehole 1 cm in length). The numerical mesh uses an orthogonal grid with refinement close to the borehole, expanding geometrically to the far-field boundary at 100 m. Grid generation is automated to facilitate modifications to different borehole geometries (GRIDDER, 2012).

Smaller radius boreholes discussed in Deal and Case (1987) are simulated using a radius of 0.04 m. Figure IV.1 shows this numerical mesh exaggerated in the vertical dimension with the pressure solution after 100 days of flow mapped onto the mesh in color. Pressure in the borehole at $r=0.1$ m is fixed at 0.1 MPa while the far-field boundary (100 m) is fixed at 10 MPa.

Simulations were also performed for large radius boreholes using borehole B042 geometry with a radius of 0.38 m (Munson et al. 1990). Figure IV.2 presents pressure distributions at time 0 and 100 days. Pressures are fixed at 0.1 MPa within the borehole and 6 MPa (hydrostatic) at the far field ($x = 100$ m).

Table IV.1 Properties used for model comparisons to the analytical solutions for the unheated case

Material	Property	Value
Intact salt	Density (kg/m ³)	2190
	Specific heat (MJ/kg K)	931
	Porosity (-)	0.0075
	Thermal conductivity (W/m K)	Sect. III
	Permeability (borehole) (m ²)	0.5e-21
	Permeability (column) (m ²)	1.0e-21
Borehole (Air)	Density (kg/m ³)	1
	Specific heat (MJ/kg K)	1000
	Porosity (-)	0.999
	Thermal conductivity (W/m K)	0.03
	Permeability (m ²)	1.0e-11

In the simulations presented, the temperature of the isothermal solution was fixed to 3.0°C to force the code, which computes properties based on (P,T) conditions assuming pure water, to match the lower viscosity of brine used in the analytical work presented in Nowak et al. (1988). This highlights the need to modify the viscosity dependence in FEHM to include the effects of high concentrations of salt. This will be one of the first tasks undertaken in the next stages of the project.

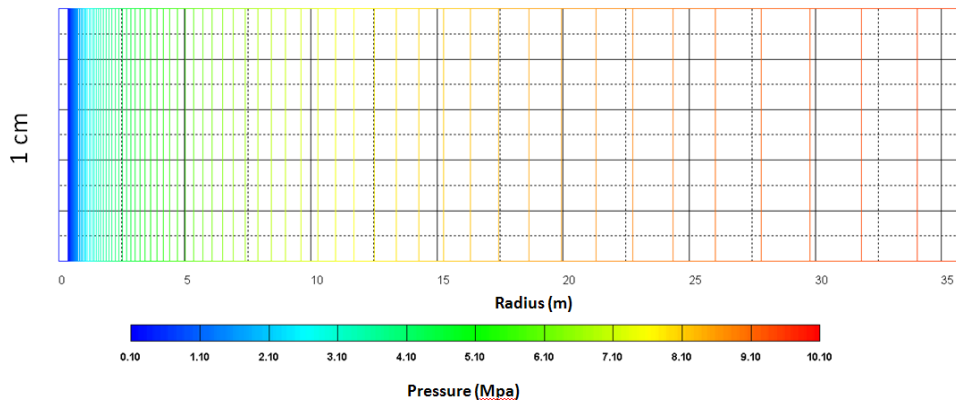
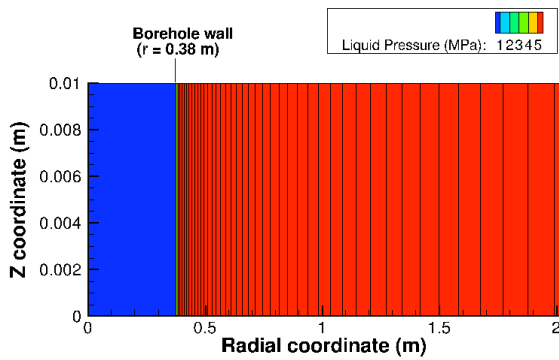
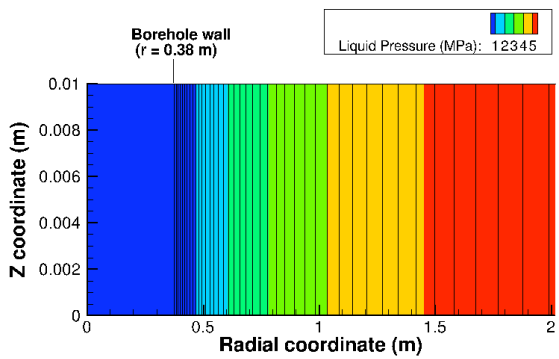


Figure IV.1 Numerical mesh for benchmarking simulations.



(a) $t = 0$ days



(b) $t = 100$ days

Figure IV.2. Pressure distributions at (a) 0 and (b) 100 days near the borehole wall for B042 nonheated simulations.

The FEHM simulation results are compared to the analytical solution above and presented in Figures IV.2 and IV.3. Table IV.1 presents the properties identified to provide flow into the borehole in the range of 5-15 g/day. For these isothermal models, the density, porosity, and permeability are relevant, whereas the thermal properties do not factor into the results. The results are plotted in dimensionless space and are able to correctly match the analytical solution (compare with Figure 1, Nowak et al. (1988)).

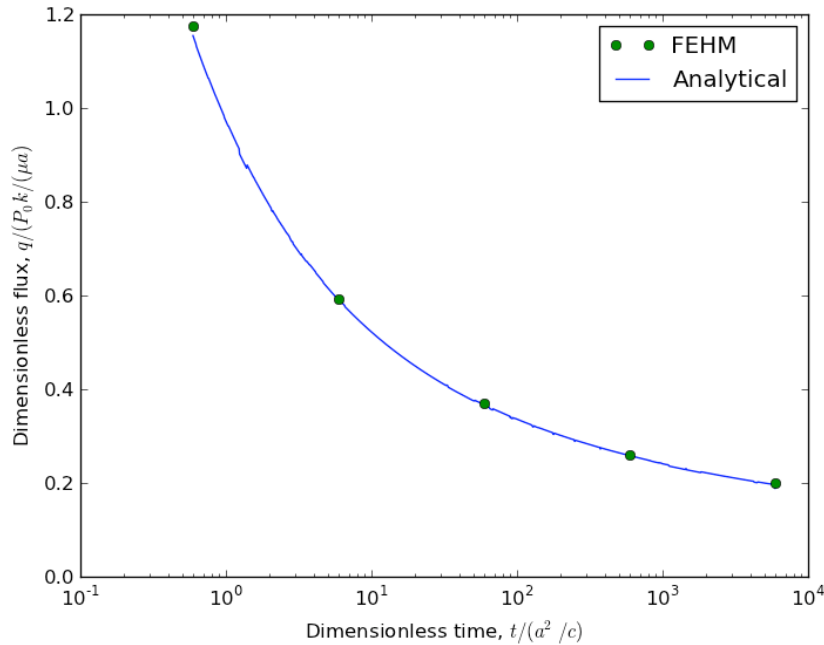


Figure IV.2 Comparison of analytical and numerical models of flux into an excavated borehole.

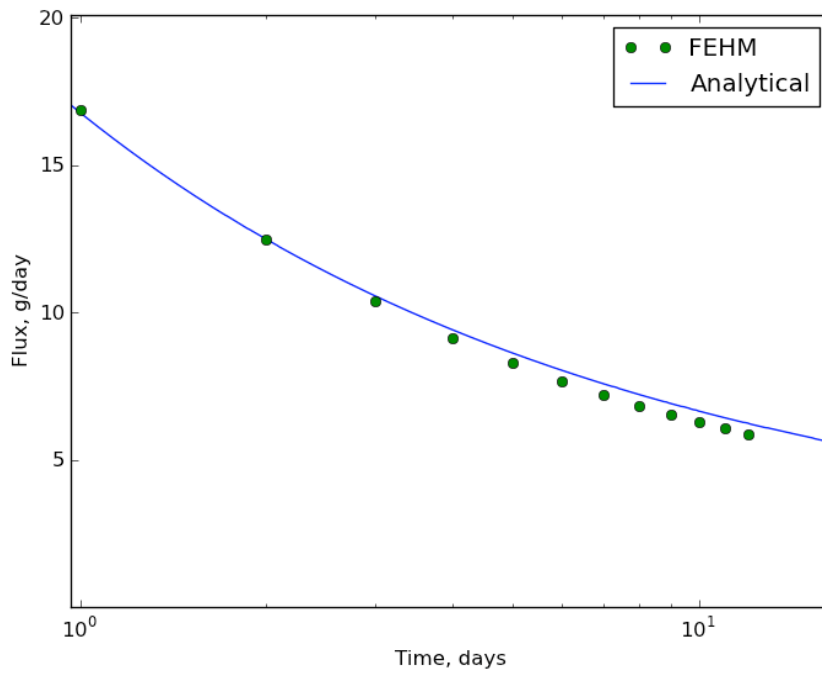
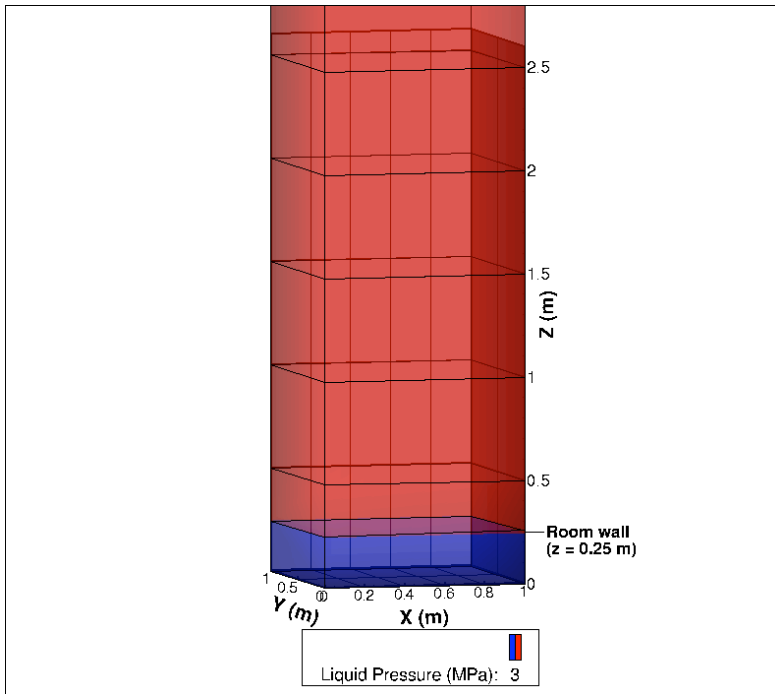
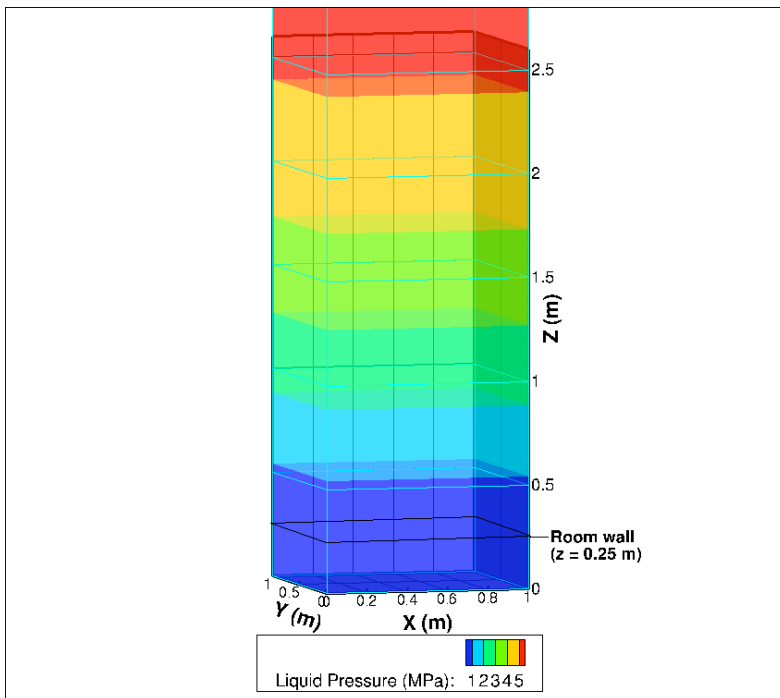


Figure IV.3 Analytical and numerical model of flux into borehole B042 in grams per day.

While assumptions required by the analytical model were imposed on the numerical model for benchmarking purposes, the numerical model does not require many of these assumptions. The numerical model can be used to explore effects of unsaturated multiphase flow and a radially limited interconnected pore network (e.g. limited to a disturbed rock zone (DRZ) surrounding the borehole).



(a) $t = 0$ days



(b) $t = 100$ days

Figure IV.4. Pressure distribution in a column of intact salt connected to an opening after (a) 0 and (b) 100 days. The interface between the opening and the intact salt is indicated as the “room wall” at $z = 0.25$ m.

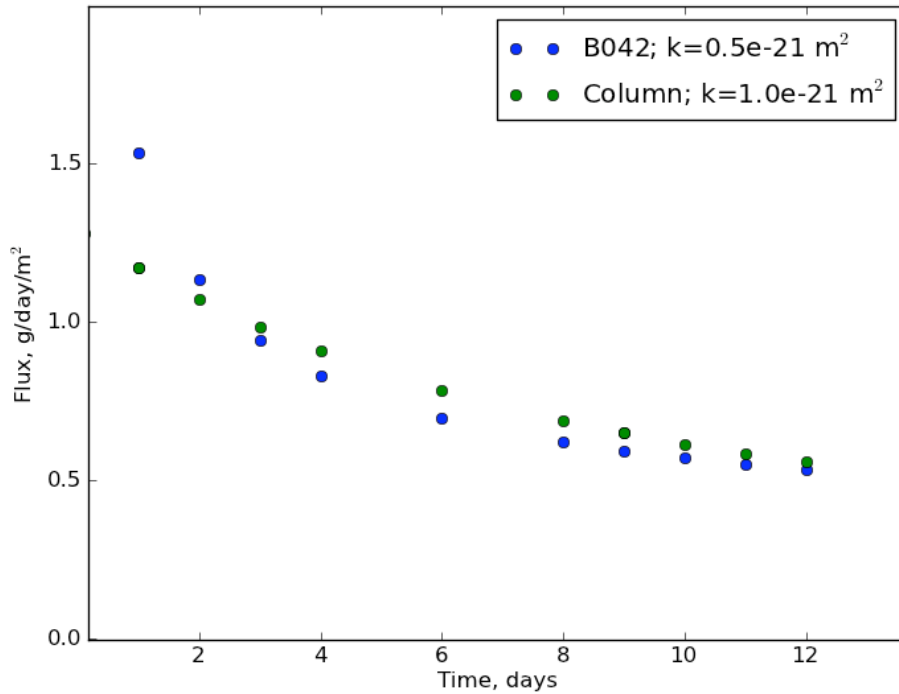


Figure IV.5. Comparison of FEHM simulated flow normalized by area into borehole B042 and a column of salt exposed to an opening on one end. Intact salt permeabilities are indicated in the legend.

Numerical simulations were also conducted to model the flow into an opening from a 1x1x100 m column of intact salt. The properties listed in Table IV.1 also apply for these simulations. Figure IV.4 presents the pressure distribution at 0 and 100 days. As in the borehole simulations, the opening ($0 \leq z \leq 0.25$ m) is held at a pressure of 0.1 MPa while the far field ($z = 100$ m) is held at 6 MPa. In order to simulate flows per unit area similar to the borehole during the first two weeks after excavation, a slightly higher permeability of 1.0×10^{-21} m² was required. This is likely due to fact that the column does not have the radially convergent flow of the borehole.

b. Heated Analytical

Nowak et al. (1988) present an analytical model of flow to a heated borehole considering the porous media as a linearly elastic skeleton. The basis of the model is the diffusion equation defined as

$$\frac{\partial p}{\partial t} - c\nabla^2 p = b' \frac{\partial \theta}{\partial t},$$

where p is the fluid pore pressure, c is the fluid diffusivity, b' is a source coefficient, θ is the temperature and t is time. The fluid diffusivity c depends on permeability, fluid viscosity, and the elastic properties of the fluid and solid.

For conduction-dominated problems, the solution of the pressure diffusion equation must be coupled with the heat equation

$$\frac{\partial \theta}{\partial t} - \kappa \nabla^2 \theta = 0,$$

where κ is the thermal diffusivity.

The initial and boundary conditions for temperature are

$$\theta(r, 0) = \theta_0,$$

$$\frac{\partial \theta}{\partial r}(a, t) = -\frac{q^h}{K},$$

and

$$\lim_{r \rightarrow \infty} \theta(r, t) = \theta_0,$$

where θ_0 is the initial temperature, a is the borehole radius, q^h is the heat flux at the borehole wall, and K is the thermal conductivity. Initial and boundary conditions for pressures are

$$p(r, 0) = p(a, t) = \lim_{r \rightarrow \infty} p(r, t) = 0$$

The solution of these equations is

$$q(a, t_*) = -\frac{kb'q^h}{\mu KR(1-R^2)} \frac{2}{\pi} \int_0^\infty \frac{\exp(-\omega^2 t_*) [\Phi J_1(\omega) - \Psi Y_1(\omega)]}{[J_1^2(R\omega) + Y_1^2(R\omega)][J_0^2(\omega) + Y_0^2(\omega)]} \frac{d\omega}{\omega},$$

where

$$\Phi = J_0(\omega)\Lambda_1 + Y_0(\omega)\Lambda_2,$$

$$\Psi = J_0(\omega)\Lambda_2 + Y_0(\omega)\Lambda_1,$$

$$\Lambda_1 = J_0(R\omega)Y_1(R\omega) - Y_0(R\omega)J_1(R\omega),$$

$$\Lambda_2 = J_0(R\omega)J_1(R\omega) + Y_0(R\omega)Y_1(R\omega),$$

and $R^2 = c/\kappa$ is the ratio of fluid and thermal diffusivities. Material property equations and typical values for WIPP are presented in Appendix A of Nowak et al. (1988). Following Nowak et al. (1988), we use a viscosity of 0.6×10^{-3} Pa s and fluid thermal expansion coefficient of 5.6×10^{-4} K⁻¹, corresponding to a temperature of 95°C, the measured temperature at the borehole wall of B042 at 100 days, the time of peak measured flux.

Figure IV.6a is a copy of Figure 3 from Nowak et al. (1988), displaying the measured cumulative brine inflow volume to borehole B042 and their simulated values using the

equations above. Figure IV.6b presents our simulated cumulative volumes calculated using the equations above and the same parameter values as listed in Nowak et al. (1988). Although the same equations and parameter values are used, it is apparent that we are unable to replicate the results from Nowak et al. (1988), where we simulate significantly less inflow. It is apparent that based on our calculations, it would require a permeability of around $1 \times 10^{-18} \text{ m}^2$ to produce flows similar those observed in B042 (i.e. crosses in Figure IV.6a). Further investigations into the formulations of these equations (e.g. McTigue (1985)) are required to uncover the source of this discrepancy. However, our numerical simulations using FEHM are able to produce similar results as analytical results of Nowak et al. (1988) (see below).

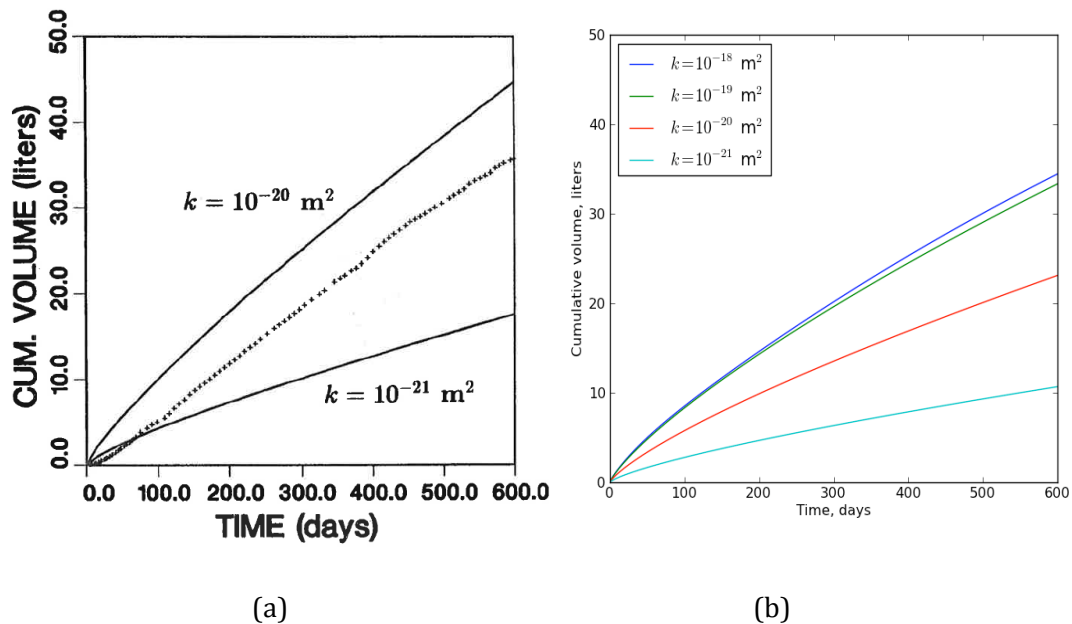


Figure IV.6 Cumulative volume of brine inflow to borehole B042. Plot (a) is a copy of Figure 3 from Nowak et al. (1988) and plot (b) is a reproduction of the simulated values using FEHM for comparison.

V. Benchmarking experimental results from the 1985 WIPP experiments

a. Isothermal phase FEHM vs Experimental data

According to Nowak et al. (1988), volumetric flux of 5-15 g/day were measured in borehole B042 prior to heating for at least two weeks. Figure V.1 presents analytical and numerical simulations of volumetric flux into B042 for 100 days, where it is apparent that the flux remains in between 5 and 15 g/day from day 1 to around two weeks. The permeability in these simulations is $0.5 \times 10^{-18} \text{ m}^2$. This indicates that permeability in B042 must be 2 orders of magnitude higher than for the smaller boreholes monitored in Deal and Case (1987) in order to simulate the volumetric flux observed in B042. Interestingly, the analytical model fits for isothermal flow fits very well with the calculated permeability that yields flows in the 5-15 g/day range. This result conflicts with the permeability estimates found in the heated analytical solution of Nowak (1988) and shows a logical inconsistency in the analytical solution that needs to be addressed. Interestingly, the analytical results that fit the experimental data obtained by LANL for the heated case yield a similar permeability ($1 \times 10^{-18} \text{ m}^2$) as we found for the isothermal part of the experiment. This suggests that the larger diameter boreholes may have higher near-field permeability than the small diameter boreholes. Such a difference could be the result of a larger damaged zone due to higher stresses and vibrations encountered when drilling large diameter boreholes.

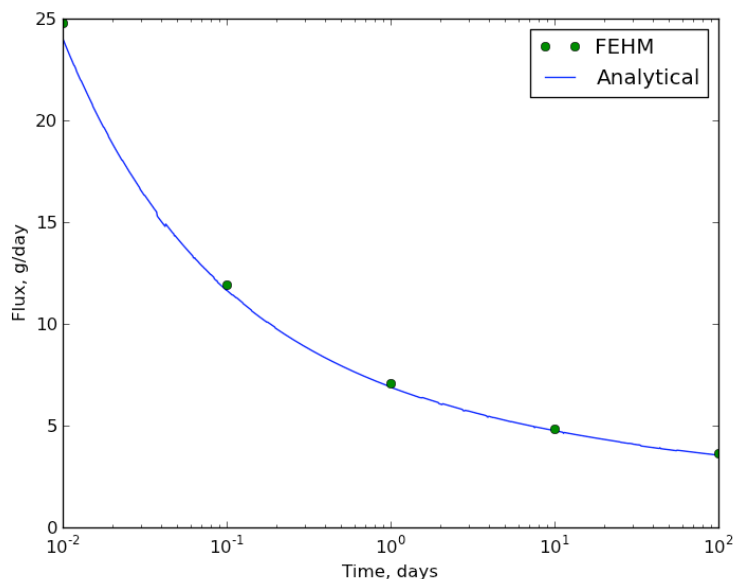


Figure V.1 Numerical and analytical simulation of non-heated volumetric flux into borehole B042 (Nowak et al. (1988)).

b. Heated phase FEHM vs Experimental data

Numerical simulations of brine inflow to a borehole in salt were performed using FEHM. In these simulations, the borehole is filled with crushed salt as described in Munson et al. (1990). Stress effects due to temperature and pore fluid pressure changes are taken into account by variable porosity and permeability. Currently, FEHM has a linear and nonlinear model (Gangi “bed of nails” model; Gangi, 1978) to account for these effects. The Gangi model for stress dependent properties was used for the borehole simulations (Gangi, 1978) where

$$\phi = \phi_0 \left[1 - \left(\frac{P_c}{P_x} \right)^m \right]$$

and

$$P_c = \sigma - P - \alpha E \Delta T,$$

where ϕ is the porosity, ϕ_0 is the initial porosity, P_c is the closure stress, P is the fluid pressure, σ is the *in situ* stress, α is the coefficient of thermal expansion of the rock, E is the Young’s modulus, ΔT is the temperature change in the rock, and P_x and m are fitting parameters. Young’s modulus is related to bulk modulus (K) and Poisson ratio (ν) as

$$E = 3K(1 - 2\nu)$$

Changes to permeability due to stress and temperature are modeled as

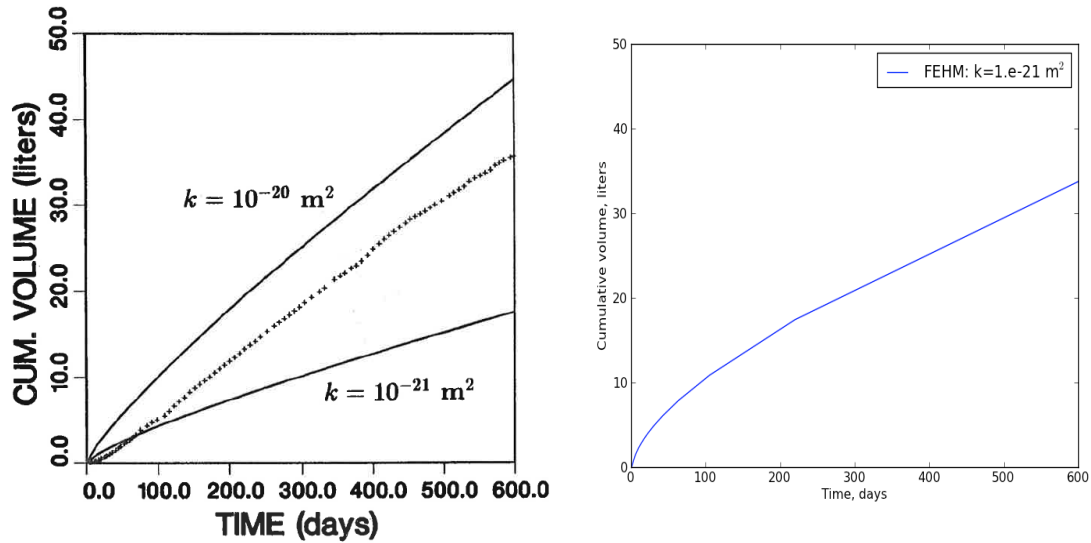
$$k = k_0 \left(\frac{\phi}{\phi_0} \right)^3,$$

where k is the current permeability and k_0 is the initial permeability. The use of the Gangi model is limited to saturated conditions in FEHM. In this initial study, these assumptions and constitutive models were adopted for convenience, so that the principle focus of the modeling, the simulation of water migration processes, could be examined; additional stress models will be incorporated in FEHM for multiphase simulations for this project.

Figure IV.2 presents the numerically simulated cumulative brine inflow into borehole B042 using FEHM. Achieving the plotted volumes required setting the permeability to $1.0 \times 10^{-21} \text{ m}^2$ and reducing the solid expansivity by around 20 times its reported value ($1.2 \times 10^{-4} \text{ K}^{-1}$; Nowak et al. (1988)). Table V.1 presents the properties used in these simulations.

Table V.1 Properties values used for model comparisons with previously published solutions for the heated case

Material	Property	Value
Intact salt	Density (kg/m ³)	2190.0
	Specific heat (MJ/kg K)	931.0
	Porosity (-)	0.01
	Thermal conductivity (W/m K)	Sect. III
	Permeability (m ²)	1.0e-21
	Gangi model parameter <i>m</i>	1.0
	Gangi model parameter <i>P_x</i>	50.0
	In situ stress (MPa)	15.0
	Solid bulk modulus (GPa)	23.5
	Solid expansivity (K ⁻¹)	5.1e-6
EDZ	Density (kg/m ³)	2190.0
	Specific heat (MJ/kg K)	931.0
	Porosity (-)	0.05
	Thermal conductivity (W/m K)	Sect. III
	Permeability (m ²)	1.0e-21
	Gangi model parameter <i>m</i>	1.0
	Gangi model parameter <i>P_x</i>	50.0
	In situ stress (MPa)	15.0
	Solid bulk modulus (GPa)	23.5
	Solid expansivity (K ⁻¹)	5.1e-6
Crushed Salt	Density (kg/m ³)	1423.0
	Specific heat (MJ/kg K)	931.0
	Porosity (-)	0.35
	Thermal conductivity (W/m K)	Sect. III
	Permeability (m ²)	1.0e-21
	Gangi model parameter <i>m</i>	1.0
	Gangi model parameter <i>P_x</i>	45.0
	In situ stress (MPa)	15.0
	Solid bulk modulus (GPa)	23.5
	Solid expansivity (K ⁻¹)	2.8e-10



(a) Nowak et al. (1988)

(b) FEHM

Figure V.2 Comparison of (a) experimental and analytical results from Nowak et al. and (b) numerically simulated cumulative brine inflow using FEHM.

By comparing Figure V.2a with V.2b, it is apparent that the numerically simulated flux into the borehole is larger at earlier times than the observed or analytical flux. Attempts to reduce the initial numerically simulated flux, including allowing non-heated flux for 2 weeks and 3 months, as in the experiment (Nowak et al. 1988), proved unsuccessful in reducing the initial flux. It is important to note that the analytical model also has elevated flux into the borehole at early time. Nowak et al. (1988) postulate that this discrepancy is due to the delay of the system to the heater during the experiment. For the numerical simulations, the cause of the discrepancy between measured and numerically simulated inflow may be due to the use of the Gangi model. The feedback on permeability in the Gangi model does not allow modeling the cracking of salt at a threshold pore fluid pressure as the temperature increases. Refinements to the stress dependent permeability are thus a critical need in the next phase of the LANL brine flow modeling. These refinements will explore the potential to account for stress effects in a continuum model. Explicit modeling of crack propagation is another possible area of exploration.

Figures V.3 and V.4 present the numerically simulated temperature and pore fluid pressure after heating borehole B042 for 600 days, respectively. Figure V.5 presents a time series of numerically simulated temperatures at the borehole wall. The wall temperature in the simulation ($\sim 60 \text{ }^\circ\text{C}$) is less than the measured value of $95 \text{ }^\circ\text{C}$. This discrepancy may be due to differences in the heater geometry from the experiment to the simulation. In the experiment, the heater radius is 0.301 m , while in the simulation it is 0.1875 m . The difference in heater radius is due to the node spacing of the mesh and is not expected to significantly affect the simulated flow into the borehole as in both the experiment and simulation, the enthalpy source is centered on the middle of the borehole. Pressure is fixed at 0.1 MPa (atmospheric) at the nodes in the borehole adjacent to the borehole wall to allow mass outflow. Initial pressures in the heater are set to 0.1 MPa , but

are not fixed. Therefore, increased pressures are observed in the heater in Figure V.4. This is not expected to influence the flux across the borehole wall. Initial pressure in the intact salt is set to 10 MPa, between hydrostatic (~6 MPa) and lithostatic (~15 MPa) pressure at WIPP. The far field (radius = 100 m) is fixed to 10 MPa.

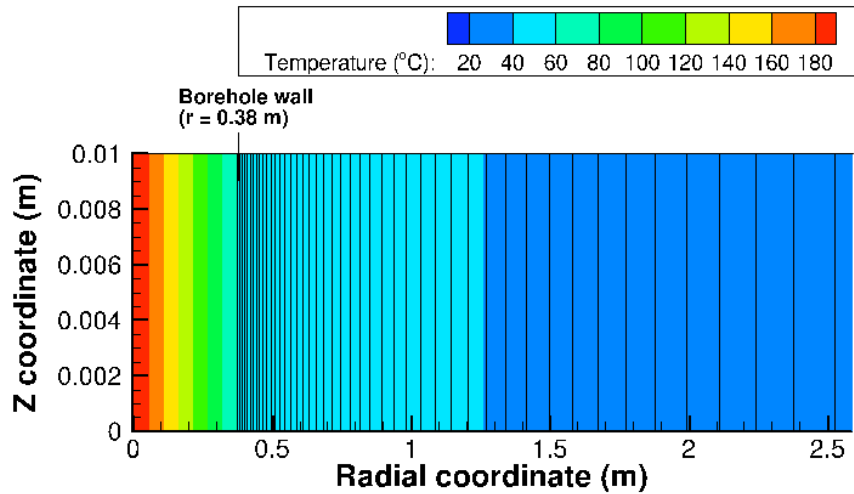


Figure V.3. Temperature profile in 2D radial simulation of borehole B042 after heating for 600 days.

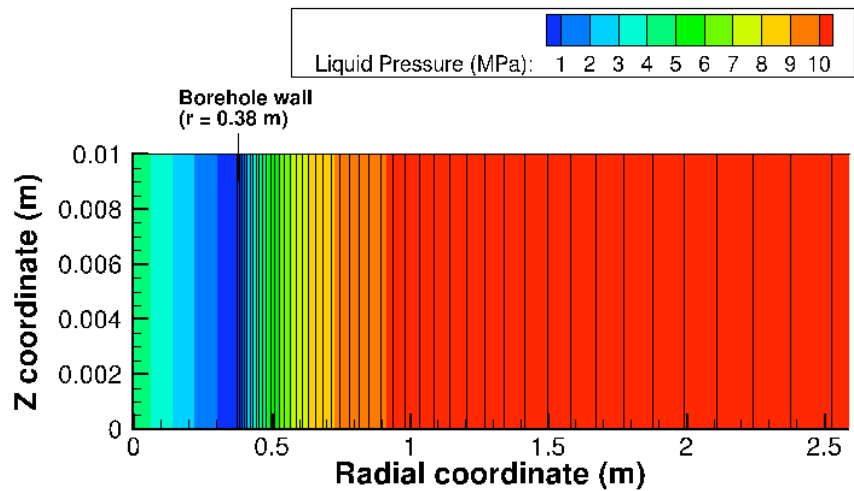


Figure V.4. Liquid pressure profile in 2D radial simulation of borehole B042 after heating for 600 days.

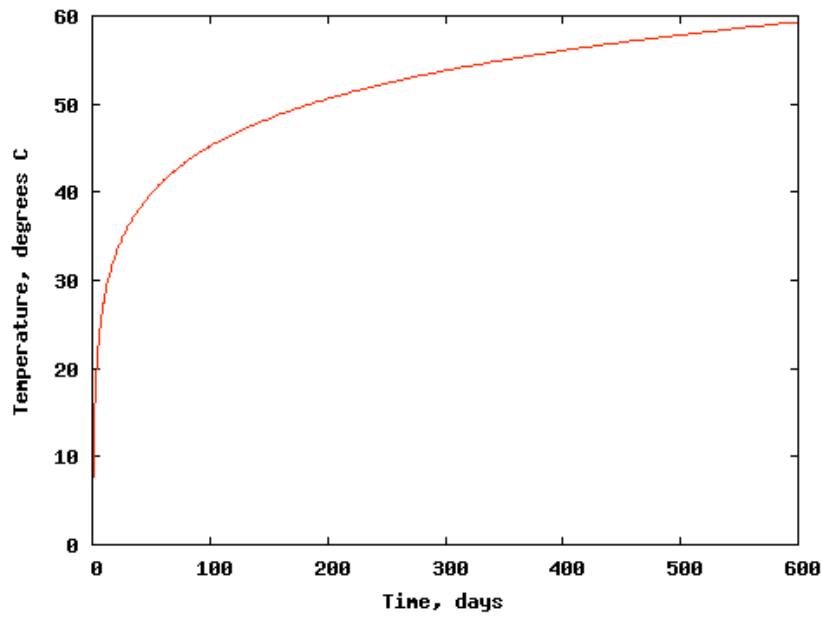


Figure V.5. Numerically simulated temperature at the borehole wall of B042 during heating.

VI. Drift scale heater tests (thermal only)

This section describes proof-of-concept calculations for a hypothetical drift scale heater experiment, using the results of modeling of brine migration to boreholes just presented as a basis for capturing the large-scale fluid movement into the drift. Such a heater experiment would demonstrate how heat-generating nuclear waste might perturb the background temperature and water profiles within the repository. In this initial study, the goal is to build a capability that would serve to predict the thermal evolution and liberation and fate of water during the initial phase of waste emplacement, and to assist in the design of field scale heater tests to study that behavior. In this section, we present calculations using heat flow only, with no water present. Following this section, a series of simulations using an approximation of the seepage flow from intact salt into partially saturated run-of-mine salt is presented. Thus, this model configuration simulates an experiment testing the in-drift disposal concept of placement of a waste package (or heater in the case of a field demonstration) on the floor of the drift, and covering it with run-of-mine salt as backfill for radiation shielding. The results take the benchmarked FEHM brine inflow results and build them into the drift scale heater simulations with a goal of better understanding of possible water migration during such thermal testing.

We begin with a discussion of the heater loads that are suitable for such a test. For defense waste, data on existing thermally active waste containers from around the DOE complex suggest heat loads that could vary from less than 100 W per package to some with over 2000 W per package (Carter et al. 2012).

Civilian waste consists primarily of SNF from the nation's nuclear power reactors, stored temporarily by the utilities at the site of currently or formerly operating nuclear power plants. The Yucca Mountain EIS categorized the heat loads of disposal packages for the Yucca Mountain repository on the basis of average heat loads across a wide range of fuel burnups and ages. The analysis was designed to enable the average heat load across the repository to be represented, to specify the configuration of disposal packages to be disposed of in the repository, and to ensure that the heat loads were reasonably bounding. Given this purpose, the EIS specified a total of 4239 containers of PWR SNF with 21 fuel assemblies per container, and 2784 containers of BWR SNF with 44 fuel assemblies per container. The heat loads specified were 8800 W/container for the PWR SNF, and 6200 W/container for the BWR SNF; we call these average values the "EIS baseline values." These values mask a broad variability in the heat loads of actual SNF, some of which is much cooler. In general, SNF discharged from commercial reactors in the 1960s - 1980s has much lower burnups than fuel being produced today, a factor that, along with the longer out-of-reactor cooling period, leads to lower heat loads. For example, the 6138 MTHM of BWR SNF and 9,701 MTHM of PWR SNF produced from 1968 to 1987 was discharged with an average burnup of 21,000 MWd/MTHM for the BWR SNF and 28,000 MWd/MTHM for the PWR SNF (derived from Tables 3 and 4 of Notz, 1990). Considering the 50 years of cooling of a low-burnup, older fuel, versus an average design basis of 23-year cooled fuel with higher burnup (33,600 MWd/MTHM for BWR and 41,200 MWd/MTHM for PWR), we would expect some 21-PWR and 44-BWR packages to have heat loads at the time of disposal that are at least a factor of 0.5 lower than the design values used in the EIS, placing these packages in the range of 3100-4400

W/container. At a finer level of discretization, within the inventory of older, low-burnup fuel, there are portions with burnups much smaller even than these lower average values, implying heat loads that are lower still.

Beyond this analysis, it is possible that the consideration of a new repository might lead to a reconsideration of the number of fuel assemblies packaged in an individual disposal container. Hardin et al. (2011) examined thermal management issues associated with clay, granite, deep borehole, and salt repository disposal concepts, and concluded that for the concepts considered and our current state of knowledge on repository temperature limits likely to be used in repository design, salt is the medium best suited to enable relatively large disposal packages to be emplaced without exceeding temperature limits. However, all media and disposal concepts examined by Hardin et al. (2011) required smaller waste packages: from 1 assembly per waste container for deep boreholes to 12 or more assemblies per container for salt. Because all of the scenarios examined were for closed repository designs, heat management limitations are more severe than for the open design of the Yucca Mountain repository, which emphasized retrievability and thermal management during the pre-closure period as basic design concepts.

Given this result, it is reasonable to conclude that smaller disposal packages (with fewer assemblies per package) could be disposed of in a future salt repository, with the heat load per package scaled accordingly. For example, if the EIS baseline values for 21-PWR and 44-BWR packages are scaled to 4 and 12 assemblies, respectively, the heat loads would scale to values of 1680 W/container for 4-PWR packages and 1270 W/container for 12-BWR containers. These values fall within the range of thermal outputs for disposal packages of defense wastes.

The purpose of this discussion is to illustrate that an intermediate heat load thermal test would provide important field based evidence relevant to commercial SNF, either for older, cooler fuel, or in a disposal scenario in which assemblies are emplaced in smaller waste packages with fewer assemblies per package, or a combination of the two approaches. Thus, such a test would significantly advance the scientific basis for both defense and civilian wastes. When combined with an alcove disposal concept that optimally distributes high heat waste packages in the repository (e.g. Robinson et al., 2012), the in-drift concept covers the entire range of thermal conditions likely to be required for all defense and civilian wastes. Finally, we note that the in-drift concept would lead to significant ventilation of the drift for the time period in which the salt remains unconsolidated. During this period, perhaps lasting several decades, air flow through the system will remove significant quantities of heat and water vapor, influencing the moisture content and the thermal profiles in the heated area. Therefore, the in-drift system resembles an open repository design in which heat and moisture will be expelled from the emplacement drifts: these processes are considered to be advantageous from the standpoint of repository operations. For this reason, it is likely that fairly aggressive heat load in the drift could be accommodated, which opens the possibility of disposal of intermediate-heat wastes in the range of 500-2000W/container.

The crossover heat loads for which alcove disposal would be preferred over in-drift disposal are at present uncertain, but important information would be derived from an in-drift field test to address that issue. Finally, we note that the time period of significant air

flow in a disposal operation will be much greater than the duration of a field test, meaning that the demonstration will focus on a quantitative understanding of early-time processes important to thermal management and repository conditions that would then set the stage for predicting long-term behavior of the crushed salt and adjacent intact salt. Note that because of the focus on initial behavior, the degree to which drift closure impacts the consolidation of the backfill salt should be relatively small, thereby justifying the use of a coupled model that excludes the long-term geomechanical effects on the system. For long-term simulations, including post-closure analyses, these effects would certainly need to be included.

a. Drift scale heater (thermal only) test simulation design

A 3-D numerical mesh, shown in Figure VI.1, was created to include a section of a salt repository measuring 40 m x 40 m x 40 m. An experimental drift is located in the center of the domain, with five heaters spaced equally along the length of the drift. Run-of-mine (crushed) salt is backfilled on top of the heaters with angle of repose slopes forming on either end of the drift.

Table VI.1 Dimensions used for simulated drift

	ft	m	Simulated
heater length	9	2.7432	2.5
drift width	11	3.3528	3.5
lateral salt width	38	11.5824	11.5
length	80	24.384	25
height of crushed salt	10	3.048	3
depth below floor	10	3.048	3
above ceiling	10	3.048	3
lateral center to drift	43.5	13.2588	13
height of salt + buffer	16	4.8768	5
Access tunnel height	13	3.9624	4
Access tunnel width	16	4.8768	5
half the length of the block	40	12.192	12
solid crushed salt section N	20	6.096	6
edge of salt slope	34	10.3632	10.5

The experimental drift is centered at coordinate position (0,0,0), and surrounded by access tunnels. Dimensions of the experimental drift, crushed salt backfill, access tunnels, and other aspects of the simulations are given in Table VI.1. This table shows actual dimensions in both feet and meters followed by the approximate equivalents that were used in the simulations. The slight differences are due to approximations made for convenience in the construction of the orthogonal grid. The numerical mesh maintains 0.5 m lateral spacing around the experimental drift with the same 0.5 m vertical to 3 m above and 3 m below the drift floor (Figure VI.2 and VI.3). Five heaters, shown in both Figures VI.2 and VI.3 have dimensions of 2.5m x 0.5m x 0.5m in XYZ space.

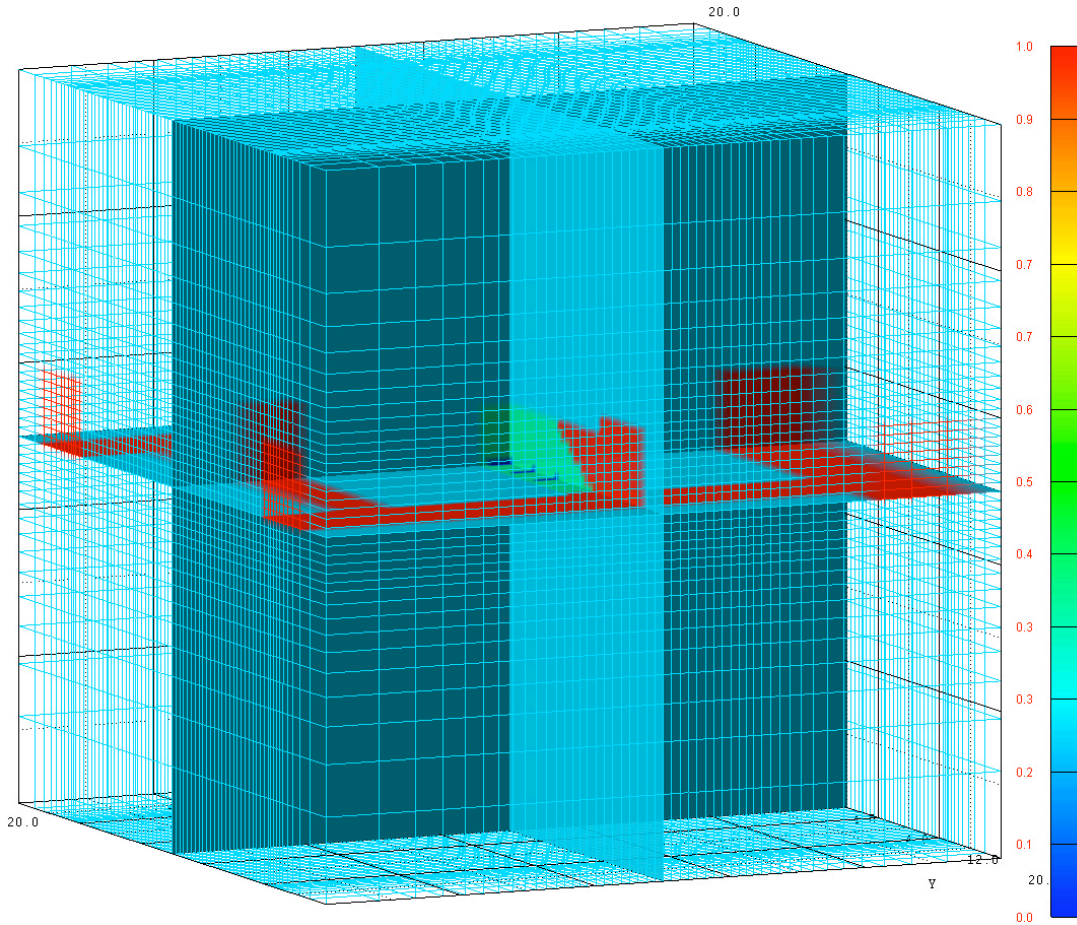


Figure VI.1 Porosity mapped onto slice planes of the numerical mesh for the proof-of-concept drift scale heater simulations. Access drifts and the outer edge of the experimental drift can be seen as red (porosity = 1.0), while the crushed salt backfill can be seen as the sloping green region with porosity of 0.35.

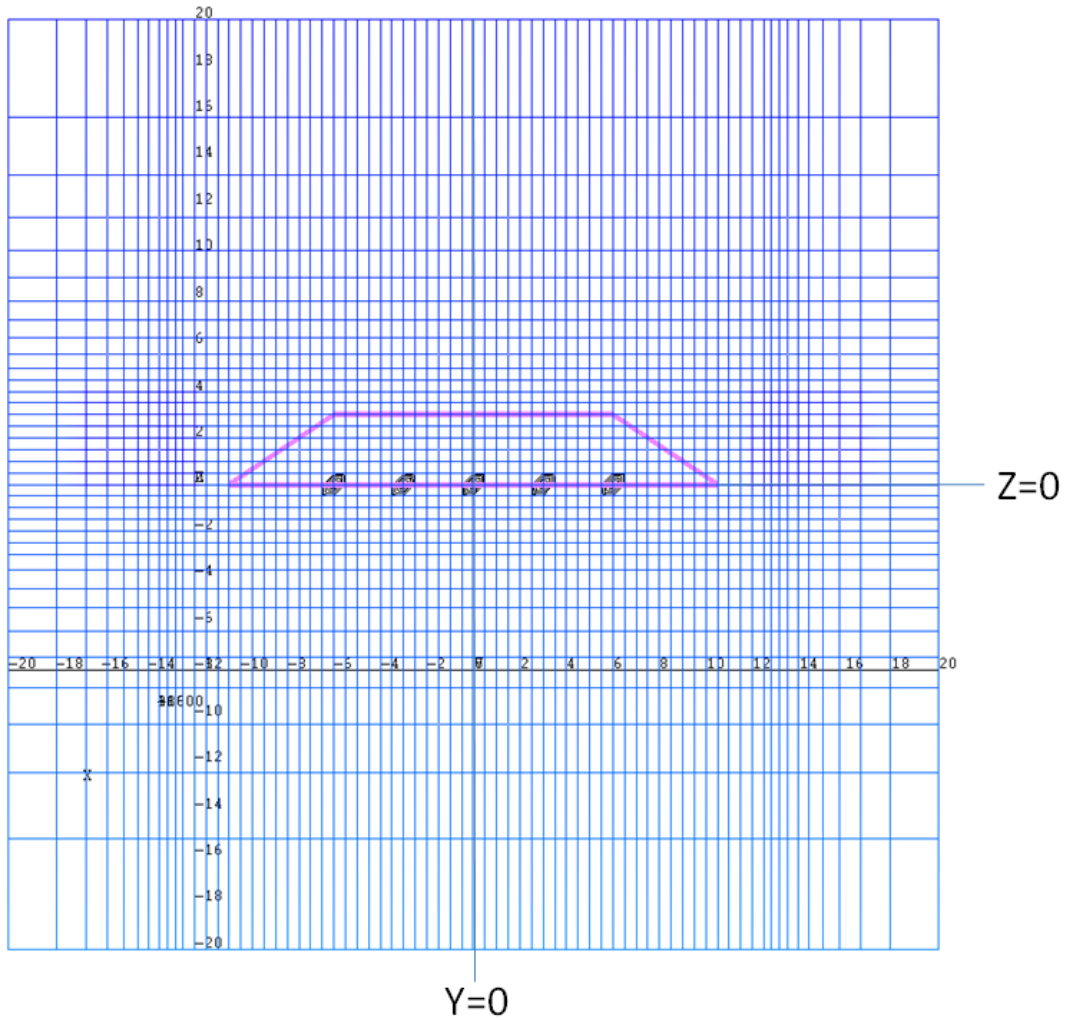


Figure VI.2 Numerical mesh on the XZ plane. The five heaters can be seen in the middle of the mesh, lying under a pile of run-of-mine salt used as backfill (pink trapezoid).

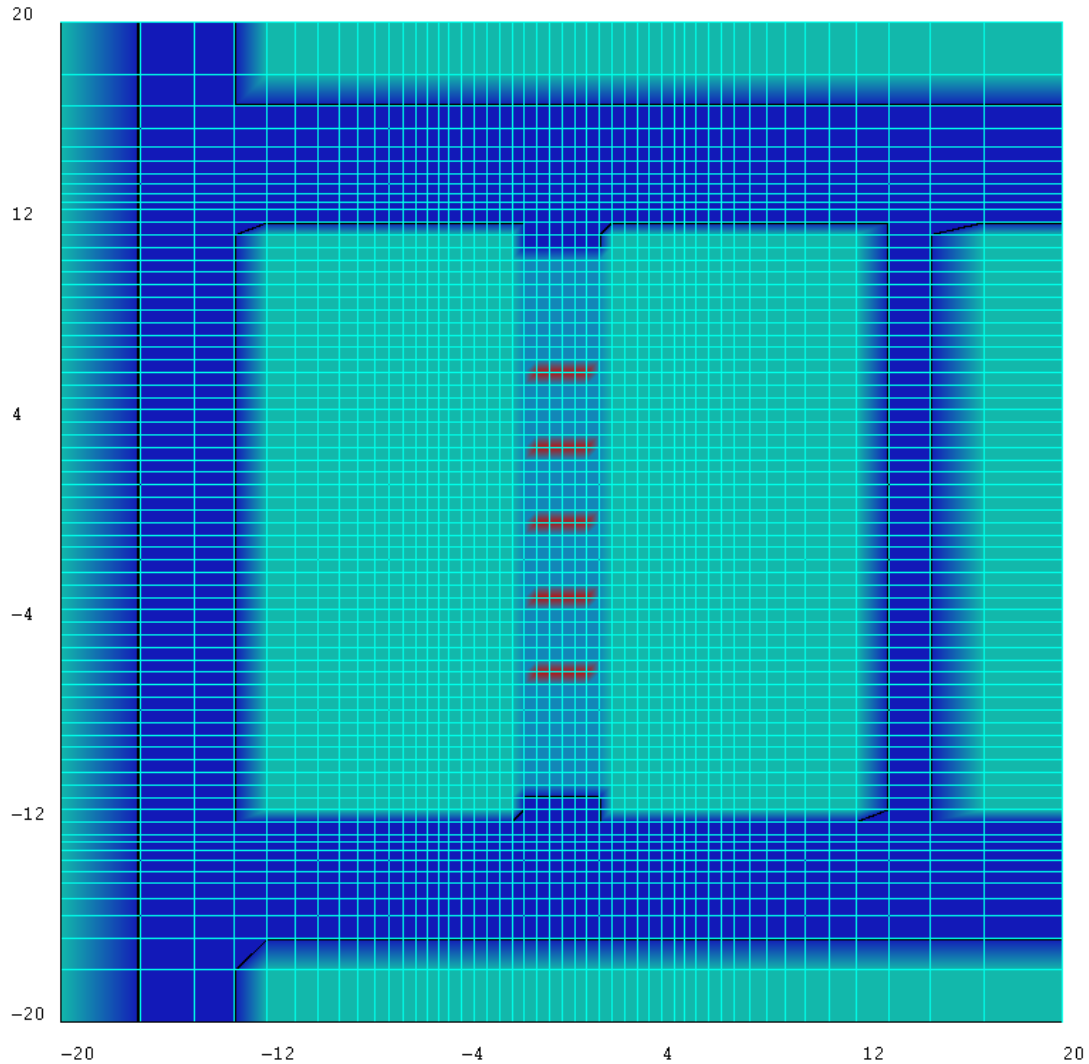


Figure VI.3 Numerical mesh on the XY plane at $Z=0$. The five heaters can be seen in the middle of the mesh. The access drifts are dark blue around the perimeter of the domain, while the experimental drift lies directly in the center and is lighter blue where the run-of-mine salt backfill is located.

b. Drift scale heater test (thermal only) simulation results

In this section, simulations are presented for a range of heating scenarios with heat loads per canister ranging from 500-2000 W, based on the previous discussion. These results are depicted in Figures VI.4 – VI.6 and discussed below.

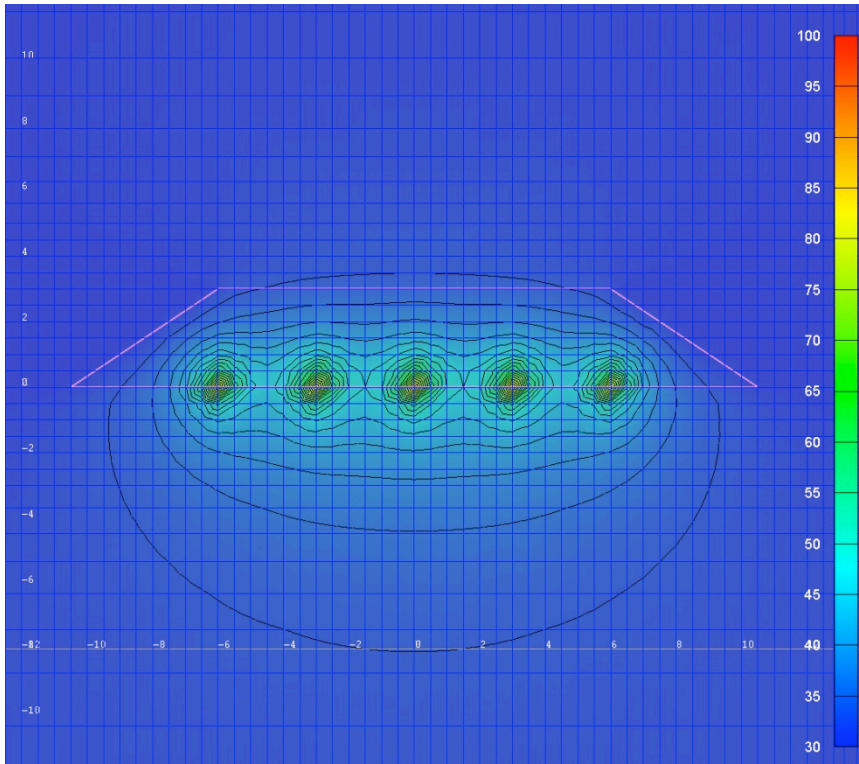


Figure VI.4 Temperature profile near steady state (1 yr) for five 500W heaters.

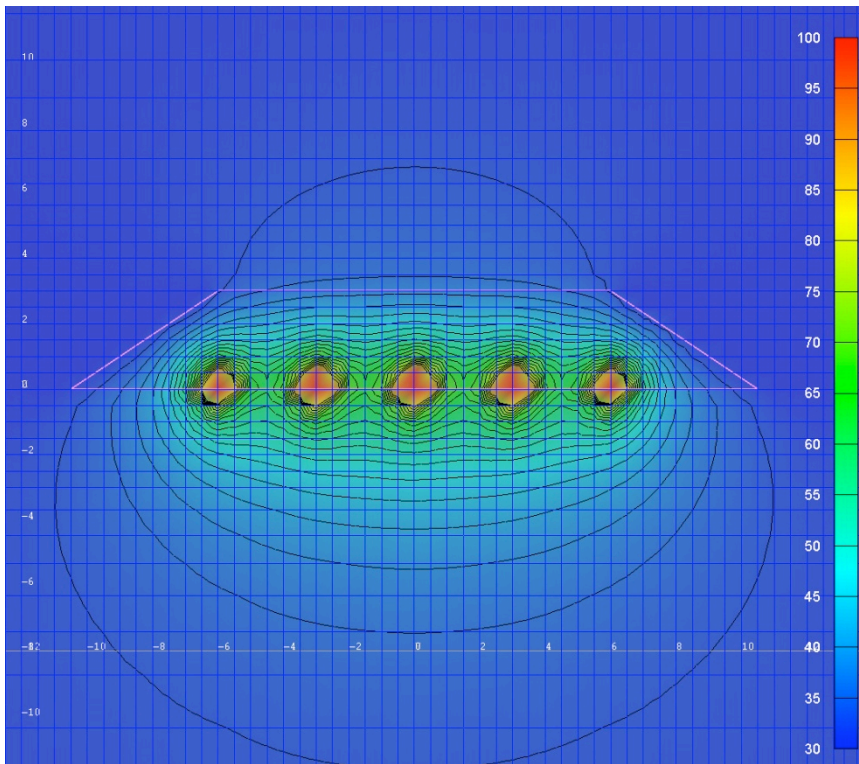


Figure VI.5 Temperature profile near steady state (1 yr) for five 1000W heaters.

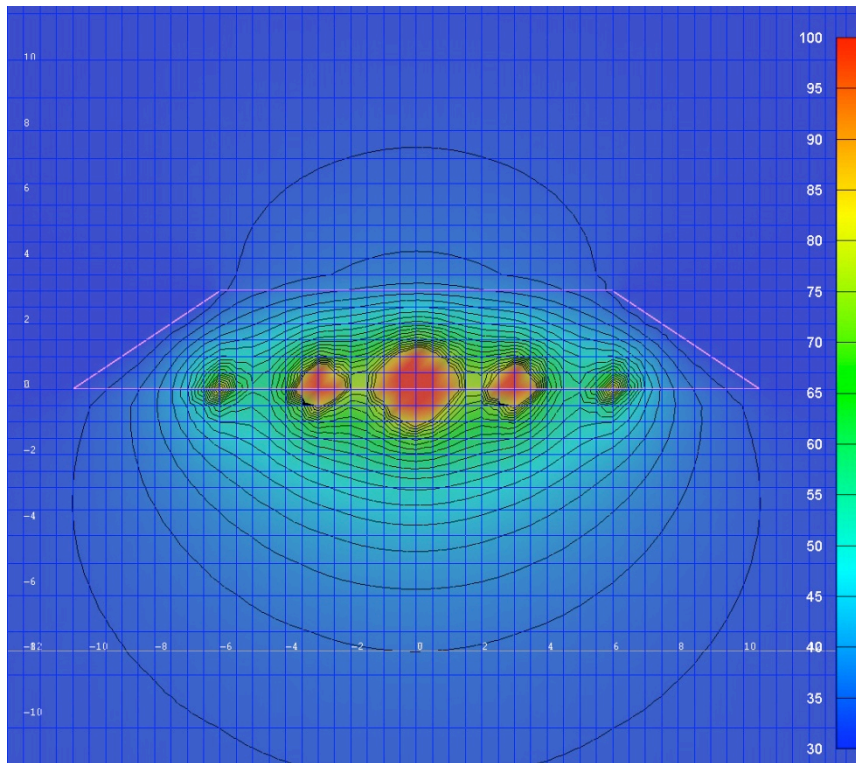


Figure VI.6 Temperature profile near steady state (1 yr) for five heaters with variable loads ranging from 2000W in the center, 1000W adjacent to the center, and 500W on the outer edges.

Temperature gradients of the sort presented in these figures serve as a prelude to understanding the potential water migration issues in either a field experiment with electrical resistance heaters or an actual repository scenario. As air moves through the porous run-of-mine salt that covers the heaters, it will become saturated with water vapor at the local thermodynamic conditions (temperature, fluid ionic strength), as long as there is liquid water present. As the air moves from a warmer to a cooler location, there will be a driving force for water condensation. Furthermore, water vapor transport and condensation could itself affect the thermal response through the heat transfer if the water vapor effects are vigorous.

Water is present initially in the run-of-mine salt, and will be augmented by seepage of water toward the drift from the surrounding intact salt. Thus, the bulk migration of water as liquid and vapor in the vicinity of the heaters (or waste packages) is subject to multiple processes, including pressure and temperature-driven flow into the drift, vaporization, and advective transport in the air phase, and possibly condensation in cooler regions due to supersaturated conditions. One of the main purposes of a field test is to demonstrate an understanding of the interplay of these processes that is sufficient to develop a quantitative model of the overall water balance during the first few years of heating. This model will serve to characterize potential changes to the rock mass that are influenced by the presence of water, and enable potential fluid interactions with the waste packages to be assessed.

VII. Drift scale heater tests (thermal/hydrological)

This section presents results from initial calculations of coupled thermal hydrological simulations intended to give a first glimpse at how moisture will redistribute in the presence of thermal loading. FEHM has been used successfully for convection studies in unsaturated media (e.g. Stauffer and Rosenberg, 2000; Stauffer et al., 1999; Kwicklis et al., 2006). We first describe a reduced numerical mesh (extracted from the mesh used in Section VI) that allows faster calculations. Next we describe unsaturated properties and initial conditions. Finally we present a several hypothetical scenarios involving different amounts of seepage water at different heat loads.

a. Drift scale heater (thermal/hydrological) test simulation design

A 3-D numerical mesh, shown in Figure VII.1, was created to include a section of a salt repository measuring 20 m x 25 m x 40 m, with 0,0,0 lying at the exact middle of the simulated experimental drift. An experimental drift is located in the center of the domain, with five heaters spaced equally along the length of the drift. Run-of-mine (crushed) salt is backfilled on top of the heaters with angle of repose slopes forming on either end of the drift. The mesh represents a half-space with a reflection boundary along $x=0$.

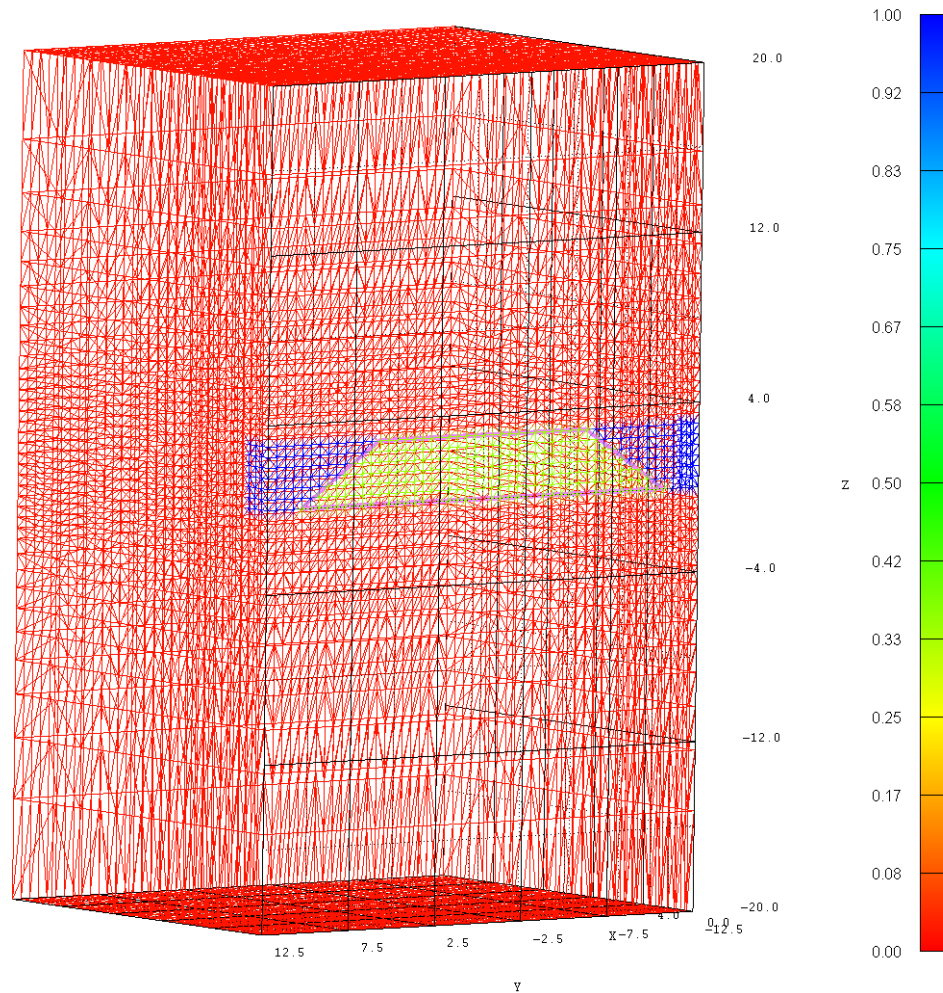


Figure VII.1 Porosity of the coupled thermal/ hydrological mesh. The drift lies along a reflection boundary resulting in $\frac{1}{2}$ the number of nodes needed. The run-of-mine backfill can be seen as yellow while the air in the drift is blue. The red surrounding material is intact salt with low porosity of 2%.

Material properties are the same as used in Table IV.1, with the exception of porosity of the intact salt which was increased to 2%. The coupled model requires the several additional properties. The simulations require that a tortuosity be used to calculate the water vapor diffusion coefficient; a standard value of 0.6 is used for this term. Unsaturated relative permeability/suction functions must be assigned for all materials. The run-of-mine salt and intact salt are assigned van Genuchten properties that lead to very low suction (large pore structure) with $\alpha=5.6 \text{ m}^{-1}$, $n=1.8$, residual water saturation of 0.0001 and maximum saturation of 1.0. The air in the drift is assigned a linear relative permeability model that generates no capillary suction. Run-of-mine salt is given a permeability of $1.0 \times 10^{-12} \text{ m}^2$, while the air is set to $1.0 \times 10^{-11} \text{ m}^2$. Modeling the air as a porous medium allows us to maintain the air at constant pressure while limiting computationally expensive convection that would occur in open air. An example input deck for FEHM is included in Appendix I for the 500W case with permeability of $6.0 \times 10^{-20} \text{ m}^2$.

Air pressure is fixed at the drift ends at a partial pressure and temperature such that the drift air maintains a pressure of 0.1 MPa and a temperature of 30°C. Thus, with no driving force for air circulation through the drift, these simulations represent the case in which air circulation is minimized, perhaps through the use of bulkheads to block or carefully control the air flow. The numerical mesh consists of 0.5 m lateral spacing around the experimental drift with the same 0.5 m vertical to 3 m above and 3 m below the drift. Background pressure in the far-field is set to 6.0 MPa at 30°C.

An initial condition is run for 50 days with no heating and the permeability of the intact salt needed to generate leakage comparable to the borehole experiments is found. For this geometry, the surface area is approximately 32x larger than the borehole experiments (350 m²), and a permeability of 6.0x10⁻²⁰ m² yields leakage of 44 kg in 50 days. This is the same order as suggested by the non-heated period of borehole B042 (5-15 g/day on 11 m²). The initial 50 day run is used to initiate simulations of heating in the drift and subsequent moisture redistribution in both the liquid and vapor phases.

The heater simulations are run for between 0.5 and 2.0 years, an amount of time likely to be devoted to such an experiment. Some of the simulations become numerically challenging as the competing flows of vapor and liquid set up a heat pipe in the crushed salt, and time step size is reduced such that running to 2 years of simulation time would require days of CPU time. Finally, thermal loads of 500W per heater to 1500W per heater are explored.

b. Drift scale heater (thermal/hydrological) test results

i. Water Accumulation in the run-of-mine backfill

To explore the impacts of heat on the movement of water in the test drift, the initial state run is restarted at time = 0 days and the heaters are turned on at constant thermal load. Because the problem uses symmetry, the heater nodes at the center of the drift are assigned ½ the thermal load of the heater nodes lying away from the reflection boundary. One of the primary diagnostics of the thermal simulations is the mass of water that moves from the intact salt into the run-of-mine salt backfill and the drift. The air in the simulation has no capillary suction, however because there are no outflows of liquid water allowed, some ponding on the drift floor occurs. This ponding accounts for less than 10% of all water flowing from the intact salt. An algorithm was written to calculate the change in mass ΔM , for different regions as:

$$\Delta M = \sum_{n=1}^{nodes} ((sat_f * \rho_f - sat_i * \rho_i) * \varphi * vol)_n$$

for each node n of the run-of-mine salt, drift, or bare drift floor; sat is the saturation, vol is the volume, φ is the porosity, ρ density of the water in the volume (a strong function of temperature), and the subscripts f and i refer to final and initial states. The algorithm is included in Appendix II of this report. Table VII.1 shows output from the model for six simulations. Total drift water includes all water in the air and run-of-mine salt, the floor water is only the bare drift floor nodes, and the run-of-mine row integrates the water found in only the run-of-mine salt. As can be seen, less than 10% of the water that seeps

into the drift ends up as ponds on the floor, while the majority of the water is pulled into the run-of-mine salt and contributes to the coupled flow.

Table VII.1 Water mass found in different regions of the model at 305 days.

	500W			1000W			1500W	
permeability (m2)	6.E-20	3.E-19	3.E-19	6.E-20	3.E-19	6.E-19	6.E-20	6.E-19
Total water seeped into drift (kg)	522	1230	2648	653	1338	2773	701	3576
Extra water in run-of-mine backfill (kg)	473	1115	2396	600	1219	2515	645	3315
Drift floor water (kg)	50	115	251	53	119	258	56	261
Percent on drift floor	0.095	0.094	0.095	0.081	0.089	0.093	0.079	0.073
% increase in run-of-mine water	0.132	0.312	0.671	0.168	0.341	0.704	0.181	0.928

ii. Base case simulation (500W with $k= 6 \times 10^{-20} \text{ m}^2$)

An initial set of calculations were done with 500W heaters to find a permeability that led to approximately the same amount of water per time per area as seen in the heated borehole experiment, B042. The rate of inflow from the experiment is 30 liters in 600 days for 11 m^2 , corresponding to 490 kg in 305 days for the simulations presented. 305 days was chosen because several of the simulations could reach this time before numerical instabilities slowed the time stepping to very low increments. The closest fit simulation is represented in the second column of Table VII.1 and yielded 522 kg of seepage water. The initial saturation and saturation at 305 days on the symmetry boundary ($x=0$) are shown in Figure VII.2. The results of this simulation are typical of all the combinations seepage and heat loads. Water is driven away from the five heaters, with saturation dropping to zero near the heaters. Water vapor is driven off and condenses as it cools away from the heaters. Once condensed, liquid water flows back toward the heaters creating an ad-hoc heat pipe in the run-of-mine salt. A map view of the saturation result on a plane sliced at $z=0.5$ (just above the drift floor) is shown in Figure VII.2C. The heaters do not dry out due to their material properties (very low permeability). Water preferentially accumulates at the end of the heater that contacts the drift wall ($x=1.5 \text{ m}$).

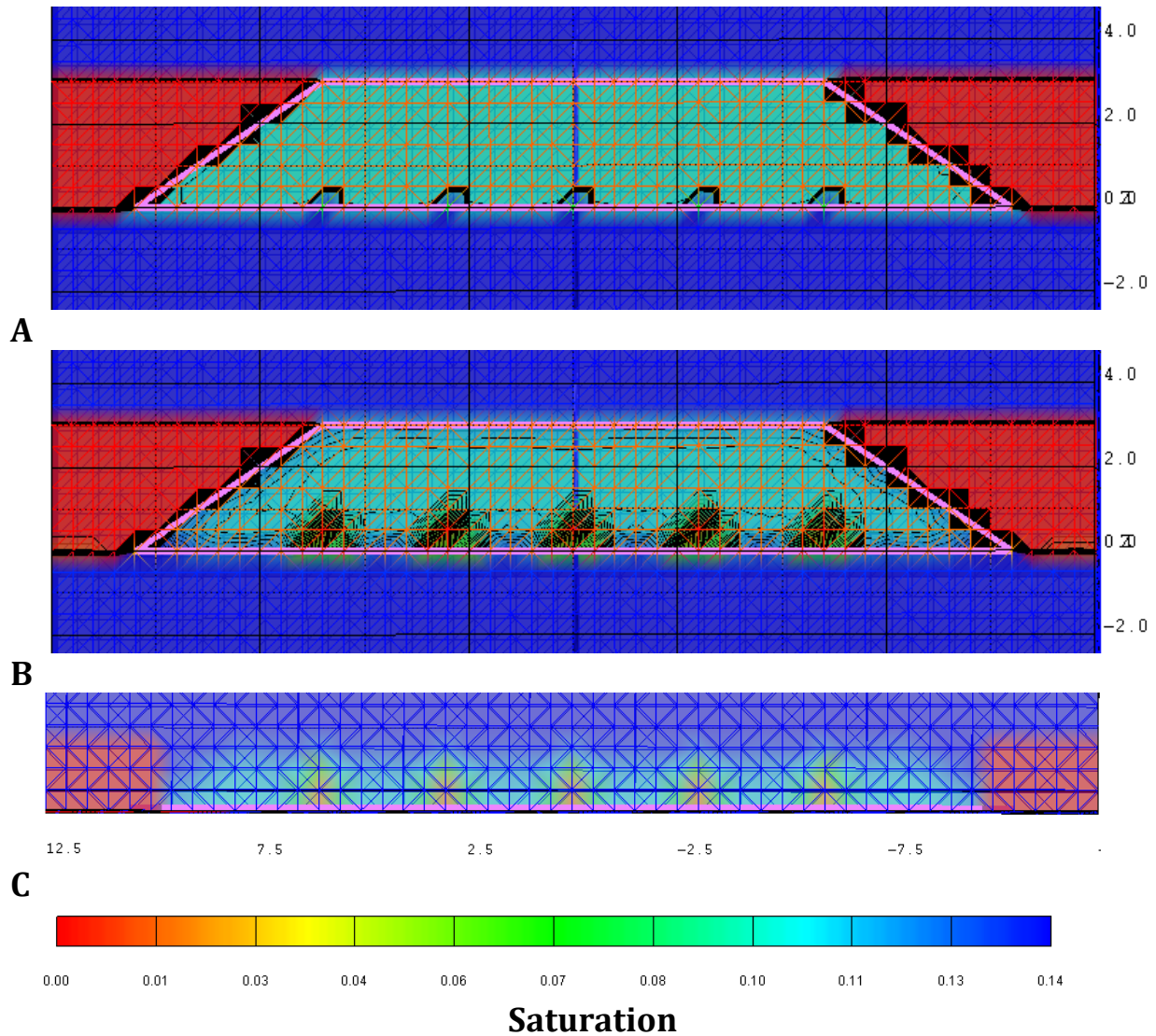


Figure VII.2 The initial saturation (A) and saturation at 305 days (B) close to the symmetry boundary ($x=0.5$). (C) shows saturation on the $z=0.5$ plane, just above the floor of the experimental drift.

The pressure profile driving flow from the background initial hydrostatic 6 MPa toward the 0.1 MPa drift is shown in Figure VII.3, for the case of the far-field boundary pressure fixed at 6.0 MPa and the saturation at 1.0. Finally, Figure VII.4 shows the associated temperature field on vertical and horizontal planes. Maximum temperature for this example is 81°C.

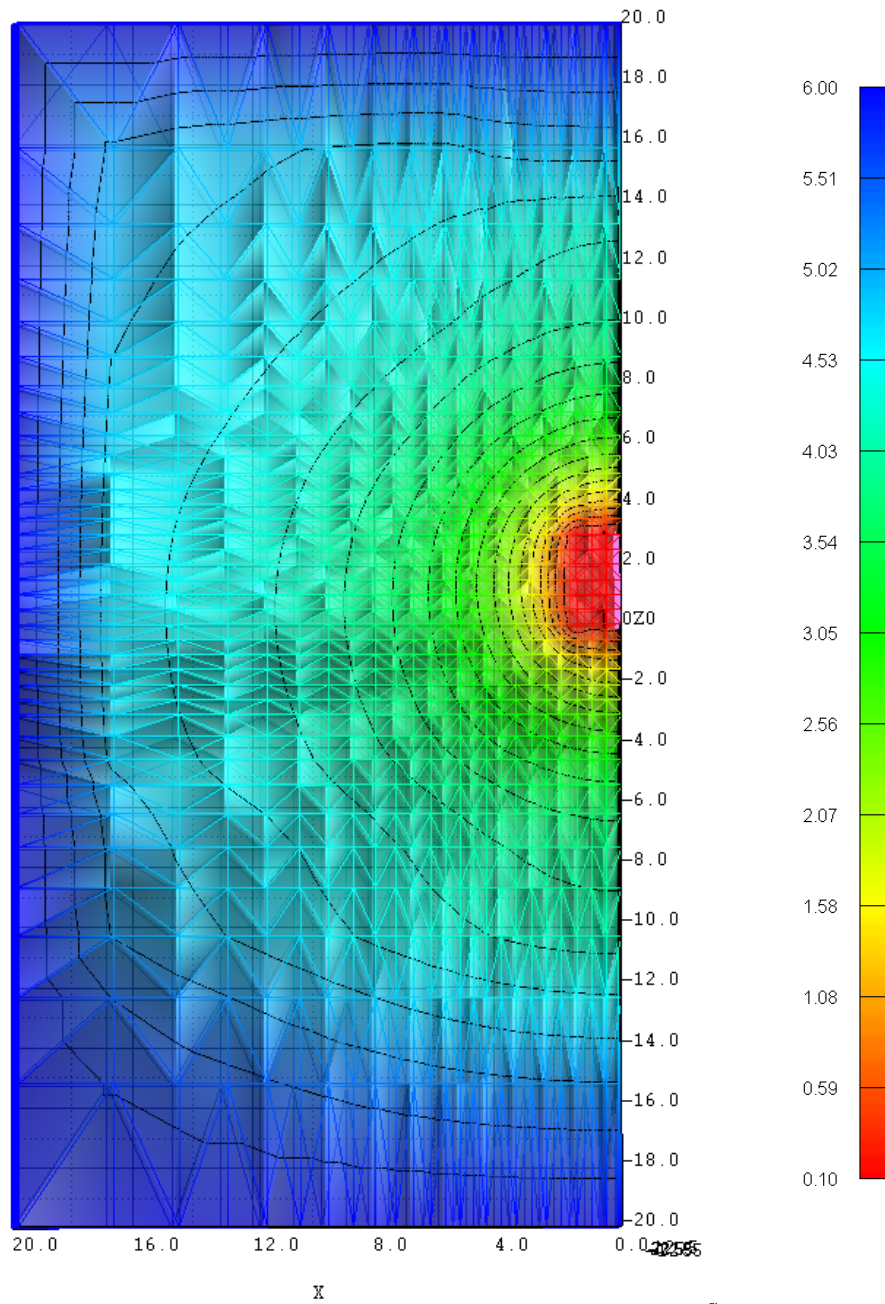


Figure VII.3 Pressure (MPa) around the 0.1 MPa drift at 305 days for the 500W heater scenario with $k=6 \times 10^{-20} \text{ m}^2$. The slice plane $y=0$.

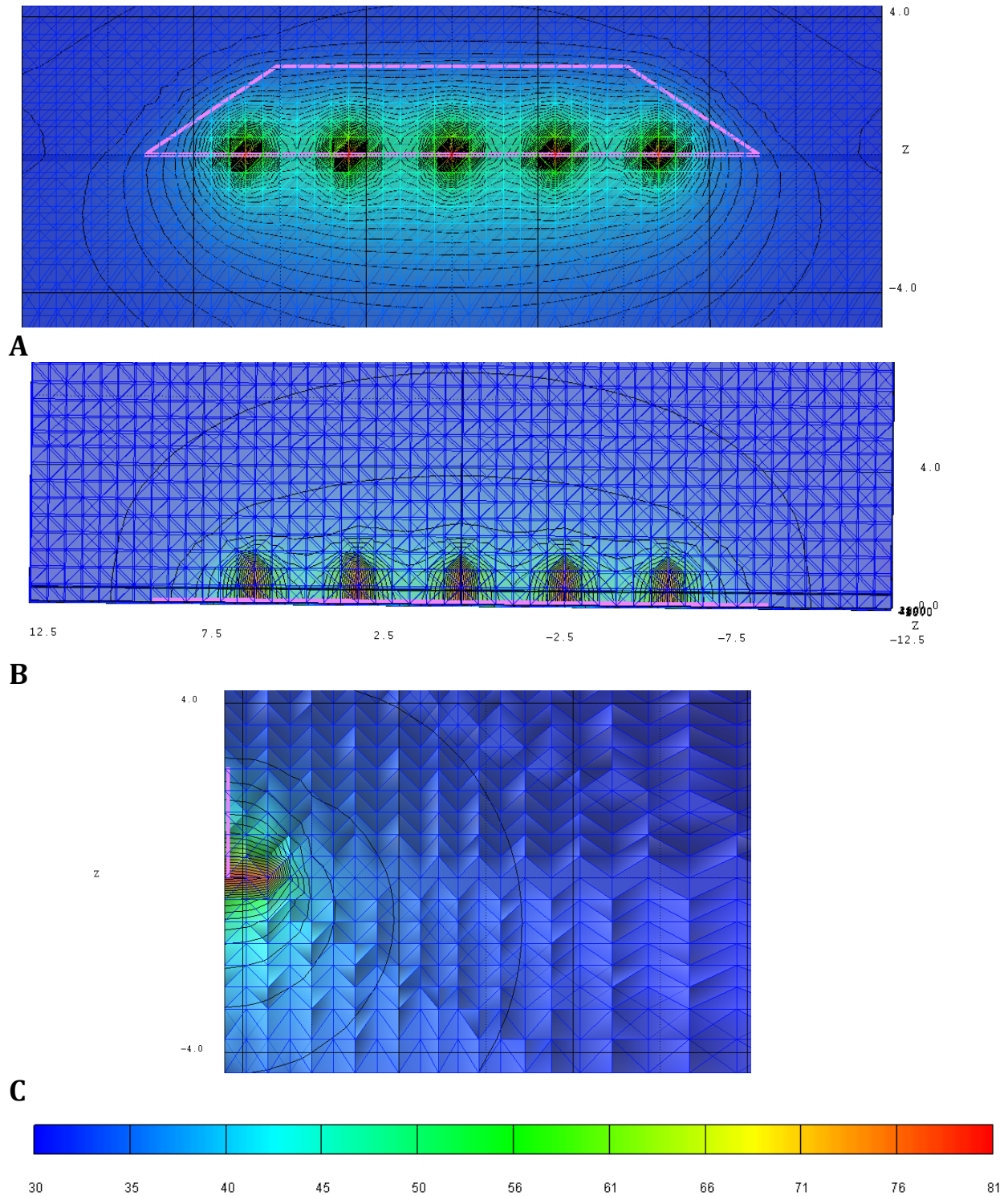


Figure VII.4 Temperature contours for the 500W case with $k=6 \times 10^{-20} \text{ m}^2$ on (A) a slice plane $x=0.5 \text{ m}$; (B) $Z = 0.0$, the floor of the drift slicing through the five heaters, and (C) $y = 0$, slicing through the center heater.

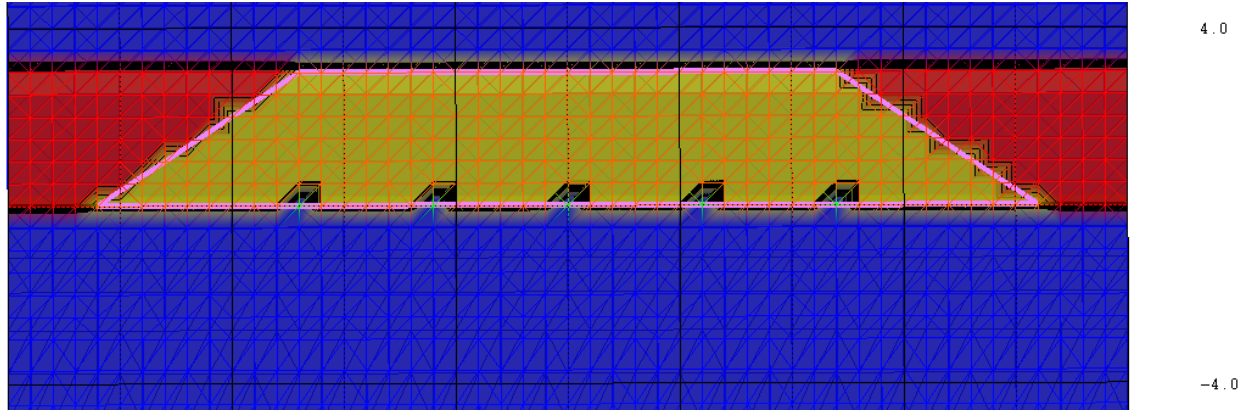
iii. Extreme case simulation (1500W with $k= 6 \times 10^{-19} \text{ m}^2$)

This section presents results from a very wet high thermal load simulation and with values summarized in the last column of Table VII.1. Figure VII.5 shows saturation slices after 1 year of heating. Dry-out is more advanced than in the 500W case, and irregular saturation contours can be seen above the heaters. Interestingly, water is accumulating at the lower tips of the backfill slopes. Water also accumulates between the heaters, with saturations being higher at $x=0$ (heater center).

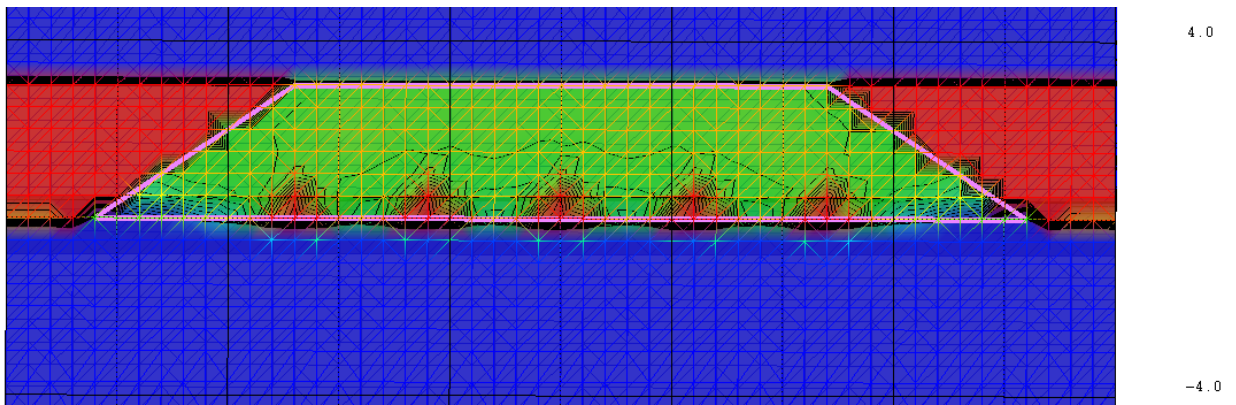
The irregular saturation contours evolve through time in a very dynamic manner. However, by two years of heating, water flow into the backfill leads to much less convective vapor transport and only the heater nodes themselves are completely dry (Figure VII.6). The total amount of water that has seeped into the backfill in two years is 8278 kg, nearly 10 m^3 . This amount of water represents a very high estimate of possible scenarios where the drift and subsequent thermal mechanical damage could lead to drainage of a water lens or large fluid filled vug (meter scale). The two year saturation for this case results in the heaters being surrounded by saturations of greater than 0.4. Figure VII.7 shows that maximum temperatures for this example are near 200 C.

Figure VII.8 shows that temperatures are above boiling (105°C) in a region around the heaters, spreading out to about a meter from the heaters. The amount of water in the problem is such that this boiling region does not lead to dry-out; water vapor condenses both vertically and laterally away from the heat source and flows back toward the heaters as liquid water. This result shows that heaters could become surrounded by fairly wet run-of-mine salt at temperatures above 100 C. Additionally, as shown on Figure VII.9, water vapor pressure in the boiling region stays quite high ($>0.1 \text{ MPa}$), meaning that the non-condensable gas has been forced out of this region and the unsaturated pore-space is filled exclusively with water vapor.

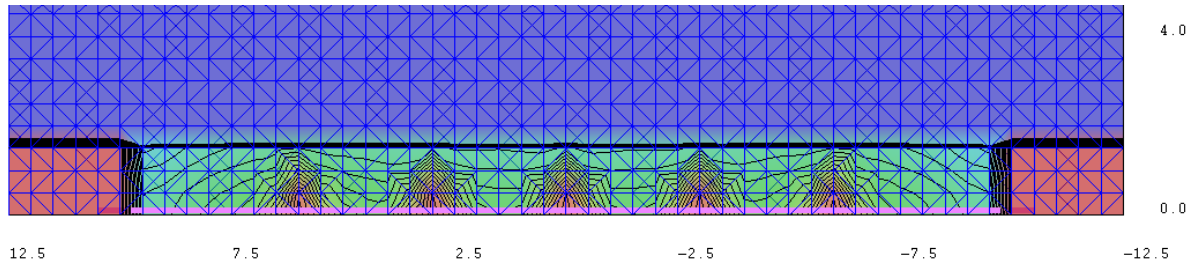
Finally, we present evidence that the coupled simulations show significant perturbations to temperature fields when compared to thermal only simulations. For this comparison, the extreme case of 1500W with $k= 6 \times 10^{-19} \text{ m}^2$ was run from the same initial saturation file (50 days) using only the thermal solution. Results from this comparison are shown in figure VII.10, which is a zoom in on the three center heaters sliced on the $x=0.5$ plane. On this figure, maximum temperature is set to 223 C. Maximum temperature in the thermal only solution is 223.2 C, while for the full air-water-water vapor simulation, maximum temperature is 196.6 after 2 years of heating. A decrease maximum temperature (in the heater) is also seen for the case of 1500W with $k= 6 \times 10^{-20} \text{ m}^2$; however for this case maximum heater temperature reaches 211.2 C. The differences in temperature fields are explained by the presence of heat pipes in the multiphase simulations. Heat pipes lead to rates of thermal transport that are higher than achieved through conduction alone. In these simulations, water vapor diffuses away from high concentration regions near the heaters (Figure VII.9) and eventually condenses back to liquid water. After condensing, some of the water flows back toward the heaters by gravity flow and along capillary pressure gradients where the cycle is repeated.



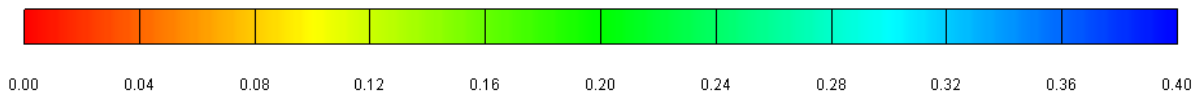
A



B

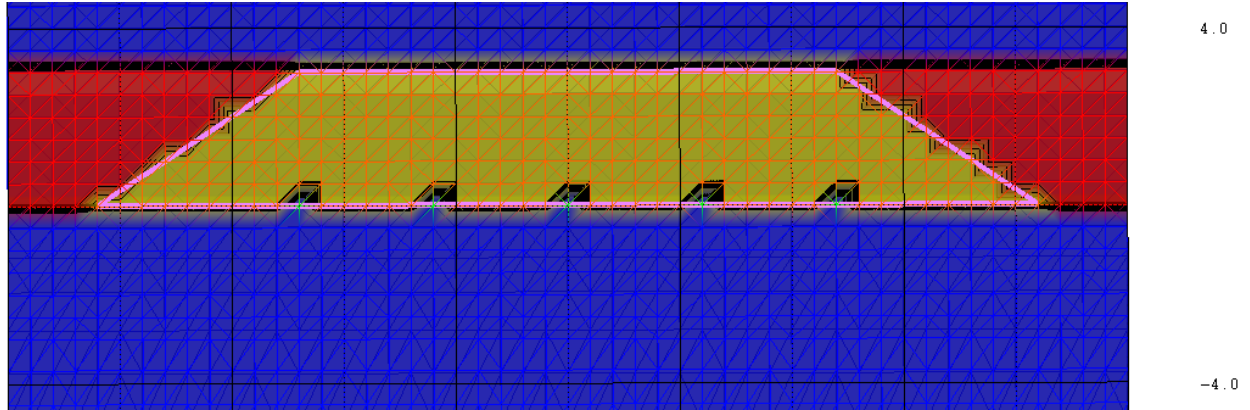


C

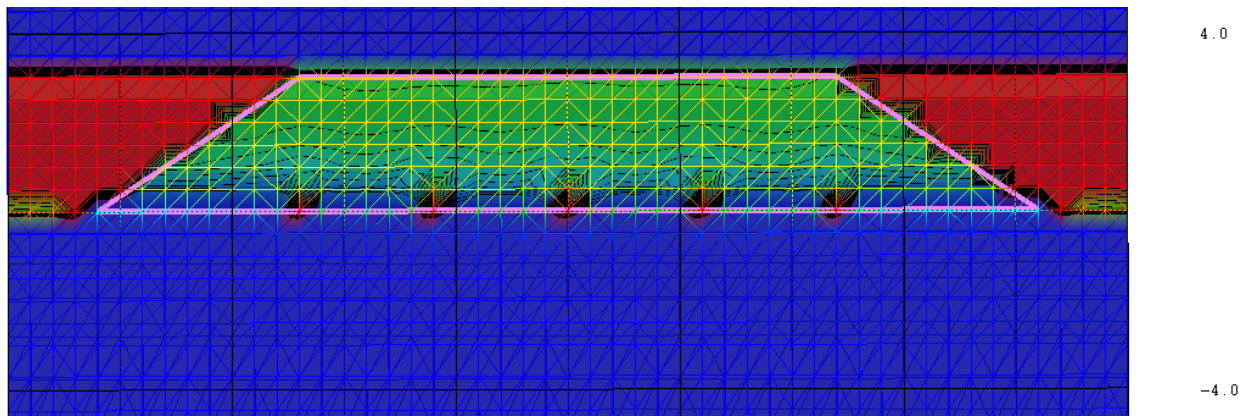


Saturation

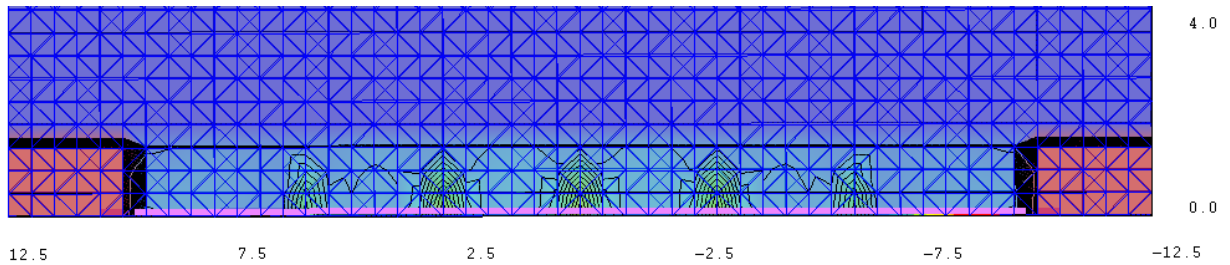
Figure VII.5 The initial saturation (A) and saturation at 365 days (B) close to the symmetry boundary ($x=0.5$). (C) shows saturation on the $z=0.5$ plane, just above the floor of the experimental drift. Results for the 1500W $k= 6 \times 10^{-19} \text{ m}^2$ case.



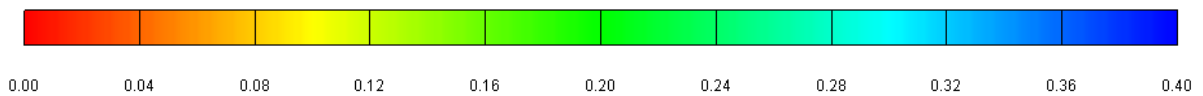
A



B



C



Saturation

Figure VII.6 The initial saturation (A) and saturation at 730 days (B) close to the symmetry boundary ($x=0.5$). (C) shows saturation on the $z=0.5$ plane, just above the floor of the experimental drift. Results for the 1500W $k= 6 \times 10^{-19} \text{ m}^2$ case.

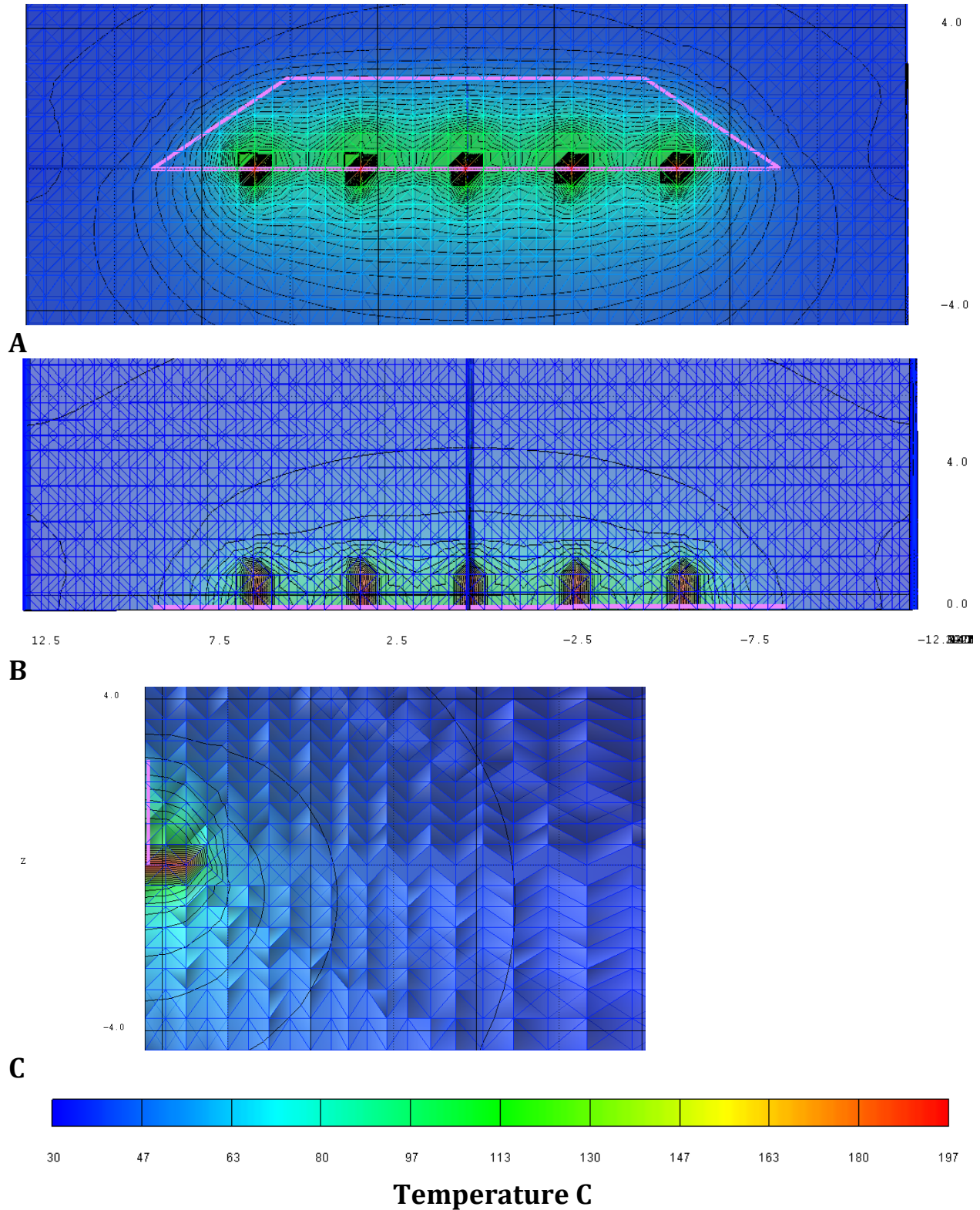


Figure VII.7 Temperature contours for the 1500W case at 730 days after heating begins, with $k=6 \times 10^{-19} \text{ m}^2$ on (A) a slice plane $x=0.5 \text{ m}$; (B) $Z = 0.0$, the floor of the drift slicing through the five heaters, and (C) $y = 0$, slicing through the center heater.

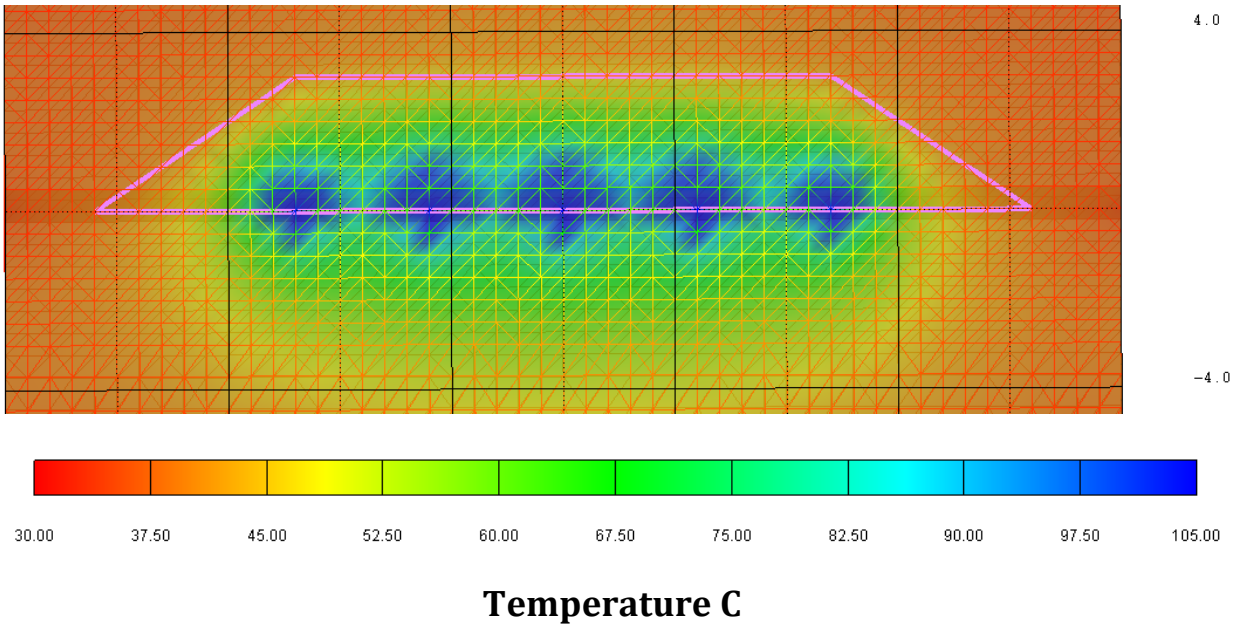


Figure VII.8 Temperature truncated at 105°C for the 1500W case at 730 days after heating begins, with $k=6 \times 10^{-19} \text{ m}^2$ on slice plane $x=0.5$.

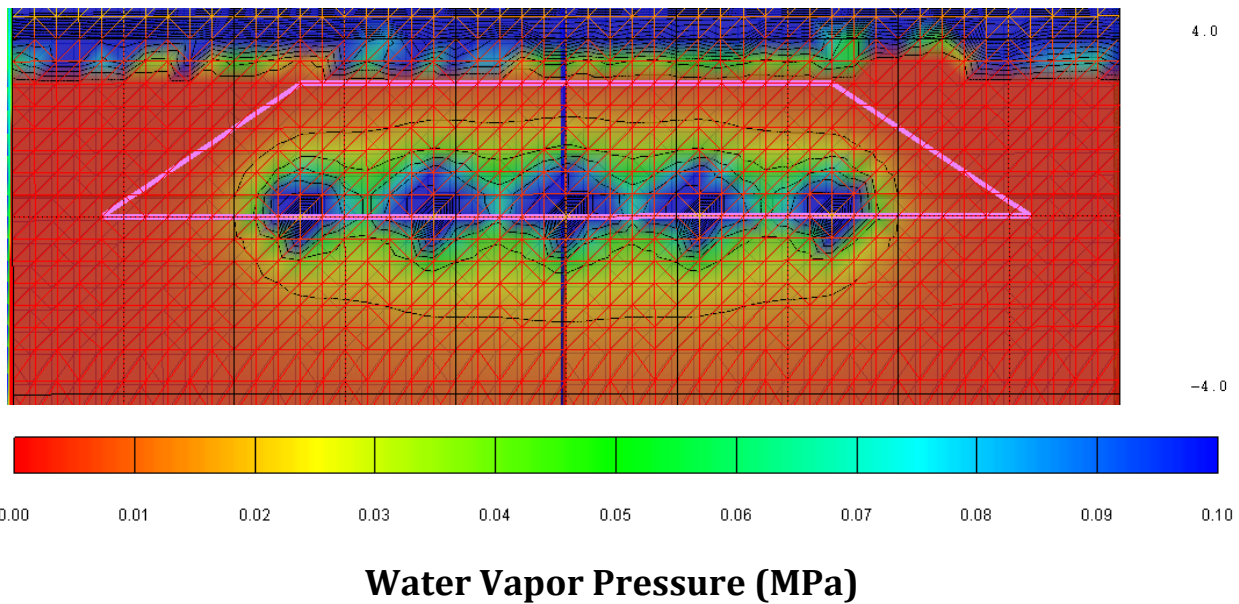
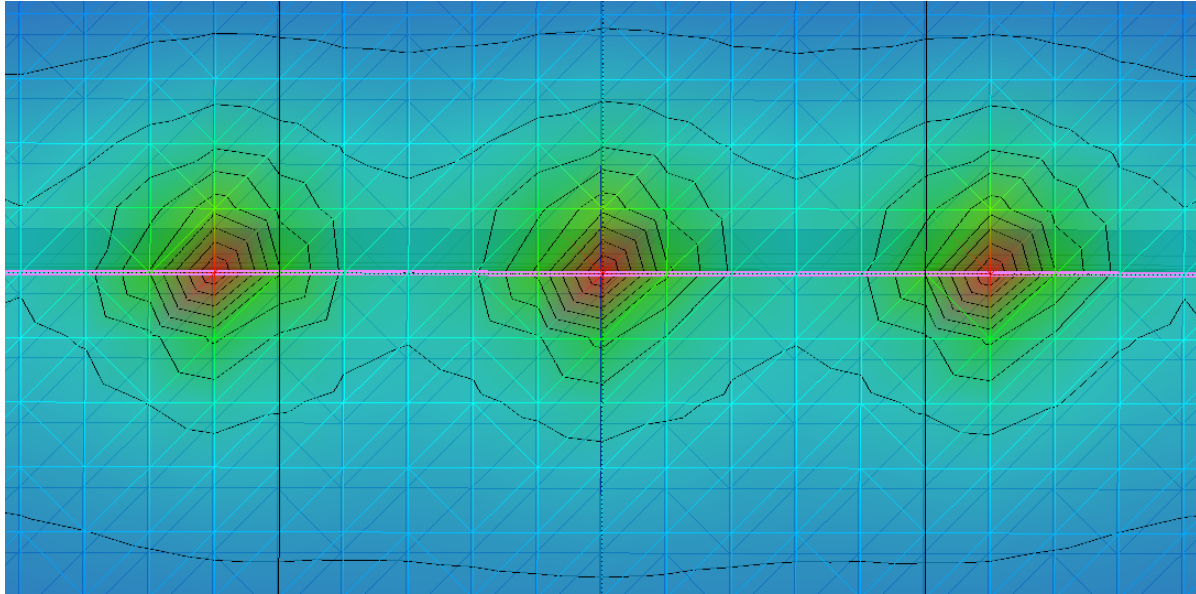
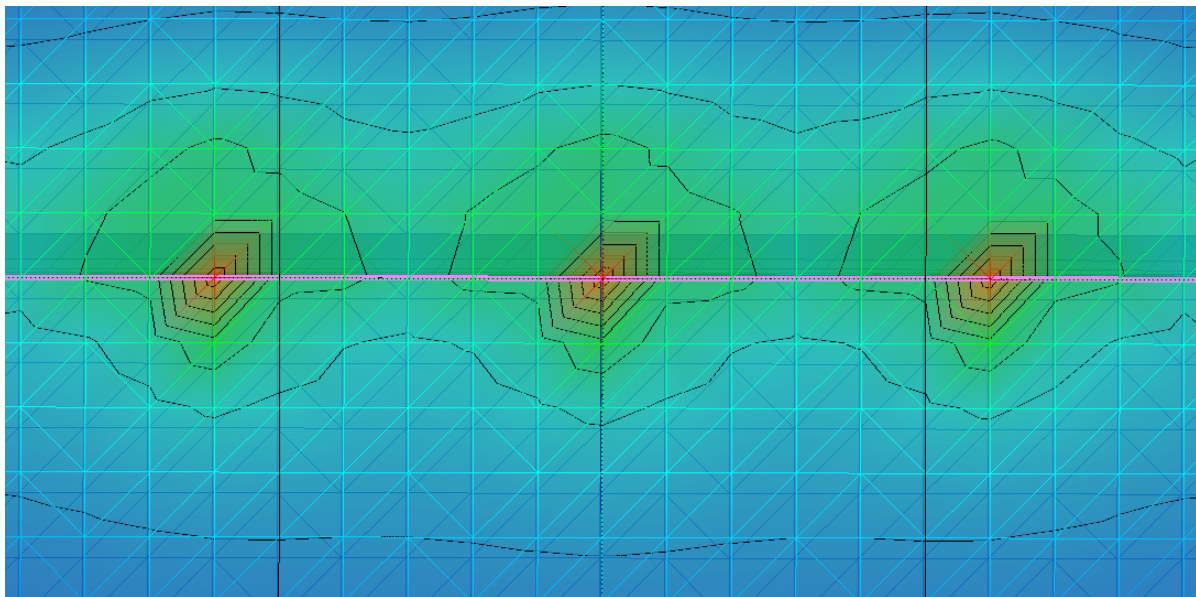


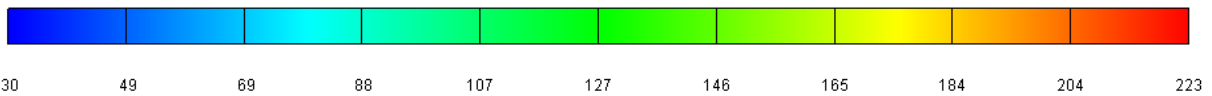
Figure VII.9 Water vapor pressure truncated at 0.1 MPa for the 1500W case at 730 days after heating begins, with $k=6 \times 10^{-19} \text{ m}^2$ on slice plane $x=0.5$.



A



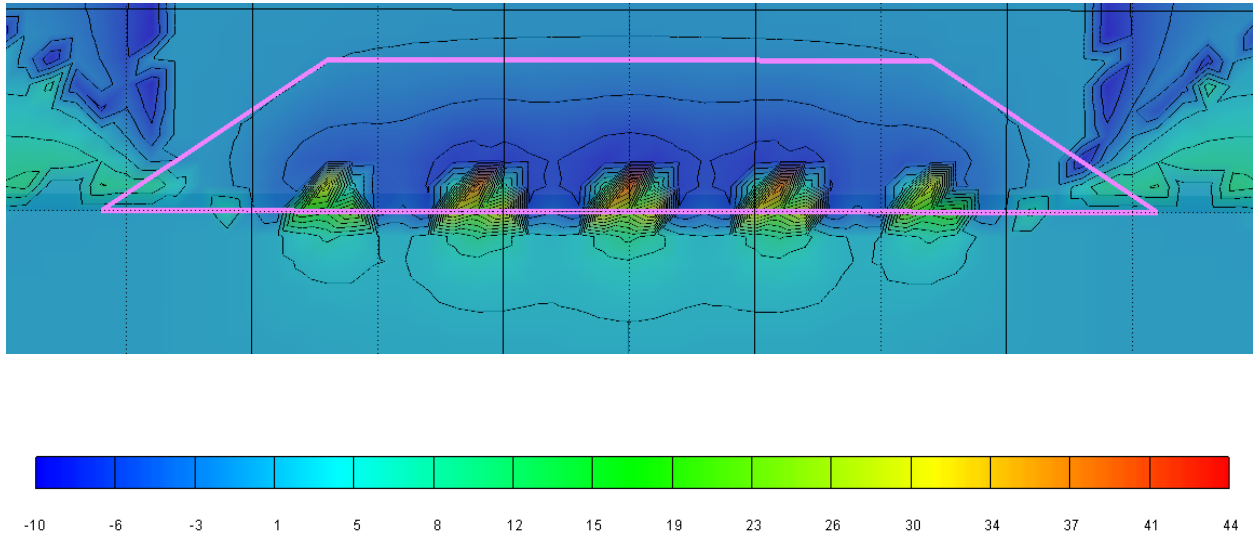
B



Temperature C

Figure VII.10 Temperature field for the 1500W case at 730 days after heating begins, with $k=6 \times 10^{-19} \text{ m}^2$ on slice plane $x=0.5$. (A) is for thermal conduction only and (B) includes multiphase heat pipe effects. Grid blocks visible as horizontal lines 0.5 m on a side, while diagonal lines show the mesh connectivity. The pink line is along $z=0$, the center elevation of the heaters.

Figure VII.11 is included to show the difference in temperature between Figures VII.10(A) and VII.10(B). Interestingly, the maximum temperature difference between the thermal conduction only versus the heat pipe simulation occurs not at the heater, but on the nodes directly above the heater at $z=0.5$ m. The maximum positive delta T for this comparison is 44 C directly above the heaters, while the maximum negative delta T is around 10 C and occurs between the heaters. This means that the heat pipe mechanism is redistributing heat vertically as well as laterally, leading to a region with low thermal gradients compared to the conduction only simulation. Such temperature homogenization could be a diagnostic when looking for multiphase impacts in a drift scale experiment.



Delta Temperature C

Figure VII.11 Temperature difference field between the conduction only case and the heat pipe case. (1500W at 730 days after heating begins, with $k=6 \times 10^{-19} \text{ m}^2$ on slice plane $x=0.5$).

VIII. Discussion and path forward

We note that the calculations presented above are preliminary, with many salt specific processes that still need to be added to the simulator to fully capture the behavior of salt, brine, in a coupled thermal-hydrological-chemical-mechanical system (THCM).

The following list of processes and ideas capture the future direction of this project.

- 1) Inclusion of a damaged zone around the drift.
- 2) Better physics of thermal expansion and permeability feedback for the intact salt.
- 3) Mineral dehydration reactions in the presence of measurable clay/gypsum.
- 4) Air circulation that could help dry out the backfill
- 5) Water release through salt decrepitation (cracking of fluid inclusions and release of included water).
- 6) Full coupling of THCM processes including permeability feedbacks caused by fracture and mineral precipitation and dissolution, fracture healing, and backfill reconsolidation under loads created by drift closure
- 7) Brine thermodynamics
 - a. Viscosity as a function of dissolved salt
 - b. Vapor pressure lowering as a function of fluid concentration
 - c. Brine density as a function of dissolved salt.

Many of these processes are already available in FEHM, however for the initial results presented here we limited to a more simple set of processes to ensure that our initial model could be used to verify that added processes are performing as expected. Thus, the results presented herein are preliminary, and the discussion represents a progress report for this ongoing project.

IX. Conclusions

The modeling presented in this report is a component of an 18-month study designed to conduct initial research and to establish the future direction for salt R&D initiatives in the U.S. The long-term goal of the coupled model development is to advance the state of coupled thermal-mechanical- hydrologic -chemical (TMHC) models used to predict the evolution of a salt-based repository after waste emplacement. The approach called for in the TMHC activity is to leverage existing computational models and tools to couple TM, TH, and C phenomena in salt under subsurface repository conditions, with a particular focus on brine accessibility and moisture transport.

To accomplish the initial phase of the coupled modeling project, the LANL FEHM computer code was used to conduct a series of hydrologic and thermal-hydrologic calculations focusing on the introduction of heat into a salt repository, and the resulting fate and transport of water under unheated and heated conditions. Benchmarking studies of FEHM against analytical solutions for brine flow to a borehole in salt show mixed results that are being further examined to determine to evaluate the source of discrepancies identified for some of the comparisons. For the isothermal case, the match is nearly perfect. For the heated case, FEHM contains permeability feedback that result in radically different results from the more simple analytical solutions. However, isothermal calculations of flow into large diameter boreholes done using FEHM and the analytical solutions both yield much higher estimates of salt permeability ($1.0 \times 10^{-18} \text{ m}^2$) than were reported by Nowak from their thermal analytical model ($5.0 \times 10^{-21} \text{ m}^2$). These higher permeabilities are more in line with values that were calculated by LANL using the thermal analytical model. The lower permeability results fit well for small diameter boreholes, and this result suggests that the larger diameter boreholes may have higher near-field permeability than the small diameter boreholes. Such a difference could be the result of a larger damaged zone due to higher stresses and vibrations encountered when drilling large diameter boreholes.

Thermal modeling of drift scale heater experiments shows that temperature perturbations will likely lead to local liquid/vapor convection over time-scales of years to decades. Simulation of drift scale heater tests over a two year period show that such convection could lead to higher liquid saturations accumulating in the relatively cool regions in between the emplaced heaters and at the lower tip of the backfill slope. These locations are likely good places for sensor emplacement to gather further data to validate models of vapor/liquid transport in a salt repository setting. Finally, comparisons of thermal conduction and thermal-hydrologic models indicates that the temperature field would be significantly different under conditions in which heat pipe effects due to boiling/condensation processes, which represent an enhanced heat transfer mechanism. This result suggests that spatial distributions of temperature alone might provide important diagnostic information regarding the mechanisms of water movement in the system during heating.

The next steps in this modeling project will be to include more realistic physical processes for stress and water source terms. The effort will benefit from interaction with both experimentalists examining brine effects, as well as those who are developing

improved geomechanics simulation capabilities. These interactions will occur in the next phase of the project.

X. References

- Carter, J. T., A. J. Luptak, J. Gastelum, C. Stockman, and A. Miller, 2012. Fuel Cycle Potential Waste Inventory for Disposition, Fuel Cycle Research & Development Report FCR&D-USED-2010-000031 Rev 5.
- Clayton, D.J. and C.W. Gable, 2009. 3-D Thermal Analyses of High-Level Waste Emplaced in a Generic Salt Repository, Advanced Fuel Cycle Initiative, AFCI-WAST-PMO-MI-DV-2009-000002, SAND2009-0633P. LA-UR-09-0089.
- J. T. Carter, A. J. Luptak, J. Gastelum, C. Stockman, and A. Miller, 2012. Fuel Cycle Potential Waste Inventory for Disposition, Fuel Cycle Research & Development Report FCR&D-USED-2010-000031 Rev 5.
- J. Crank, The Mathematics of Diffusion. Clarendon Press, Oxford, 1979, p. 87. .
- D. E. Deal and J. B. Case, IT Corporation, Brine Sampling and Evaluation Program. Phase I Report. DOE-WIPP-87-008, prepared by the Engineering and Technology Department of the Management and Operating Contractor, Waste Isolation Pilot Plant Project for the U. S. Department of Energy, June 1987. .
- E. J. Nowak, D. F. McTigue and R. Beraun, Sandia Report SAND88-0112, Brine Inflow to WIPP Disposal Rooms: Data, Modeling, and Assessment, prepared by Sandia National Laboratories, September 1988. .
- FEHM. (2012). FEHM reference list, online at http://fehm.lanl.gov/pdfs/FEHM_references_list.pdf, accessed Aug. 31, 2012. .
- A. F. Gangi (1978), Variation of whole and fractured porous rock permeability with confining pressure, Rock Mech. Sci. and Geomech. Abstr. 15: 249-257.
- GRIDDER (2012). Gridder Users Manual, (Loraine Lundquist), on-line at https://meshing.lanl.gov/gridder/users_manual.html accessed Aug. 31, 2012. .
- Hardin, E., J. Blink, H. Greenberg, M. Sutton, M. Fratoni, J. Carter, M. Dupont, and R. Howard, 2011. Generic Repository Design Concepts and Thermal Analysis (FY11), SAND2011-6202. Albuquerque: Sandia National Laboratories.
- Kwicklis, E.M., A.V. Wolfsberg, P.H. Stauffer, M.A. Walvroord, and M.J. Sully (2006), Multiphase Multicomponent Parameter Estimation for Liquid and Vapor Fluxes in Deep Arid Systems Using Hydrologic Data and Natural Environmental Traces, *Vadose Zone Journal*, 2006 5:934-950
- D. F. McTigue (1985), A linear theory for porous thermoelastic materials, SAND85-1149, Sandia National Laboratories, September 1985.
- Munson, DE, RL Jones, JR Ball, RM Clancy, DL Hoag and SV Petney. 1990. *Overtest for Simulate Defense High-Level Waste (Room B): In Situ Data Report (May 1984-February 1988) Waste Isolation Pilot Plant (WIPP) Thermal/Structural Interactions Program*, Sandia National Laboratories, SAND89-2671. .
- Notz, K.J., 1990. Characteristics of Potential Repository Wastes, First Annual International High-Level Radioactive Waste Management Conference, Las Vegas, Nevada, CONF-900406-11, April 1990.

- Robinson, B. A., N. Z. Elkins, and J. T. Carter, 2012. Development of a U.S. Nuclear Waste Repository Research Program in Salt. To appear in Nuclear Technology.
- Stauffer P.H., and Rosenberg, N.D. (2000), Vapor phase transport at a hillside landfill, *Environmental and Engineering Geoscience*, Vol. VI, No. 1, p. 71-84
- Stauffer P.H., Auer, L.H., and Rosenberg, N.D.(1997), Compressible gas in porous media: A finite amplitude analysis of natural convection, *Int. J. of Heat and Mass Transfer*, 40 (7), 1585-1589.
- Zyvoloski, G.A.(2007). *FEHM: A control volume finite element code for simulating subsurface multi-phase multi-fluid heat and mass transfer*, Report LA-UR-07-3359, Los Alamos National Laboratory.

Appendix I

```

title: Heaters in wet salt.
sol
  +1 -1
  # zone 1 = top  2 = bottom
  # zone 61-65 are the heaters
  # zone 91-95 are the drifts
  # zone 101 is the salt backfill
zonn
1
-20 20 20 -20 -20 20 20 -20
-20 -20 20 20 -20 -20 20 20
  21 21 21 21 19 19 19 19
2
-20 20 20 -20 -20 20 20 -20
-20 -20 20 20 -20 -20 20 20
-19 -19 -19 -19 -21 -21 -21 -21
3
19 20 20 19 19 20 20 19
-20 -20 20 20 -20 -20 20 20
  21 21 21 21 -21 -21 -21 -21
95
-1.75 1.75 1.75 -1.75 -1.75 1.75 1.75 -1.75
-13 -13 13 13 -13 -13 13 13
  3 3 3 3 0 0 0 0

zonn
file
/home/stauffer/Salt/Simulations/Grid02b/crushed_salt.zone
zonn
61
-1.1 1.1 1.1 -1.1 -1.1 1.1 1.1 -1.1
-6.1 -6.1 -5.9 -5.9 -6.1 -6.1 -5.9 -5.9
  0.25 0.25 0.25 0.25 -0.25 -0.25 -0.25 -0.25
62
-1.1 1.1 1.1 -1.1 -1.1 1.1 1.1 -1.1
-3.1 -3.1 -2.9 -2.9 -3.1 -3.1 -2.9 -2.9
  0.25 0.25 0.25 0.25 -0.25 -0.25 -0.25 -0.25
63
-1.1 1.1 1.1 -1.1 -1.1 1.1 1.1 -1.1
-0.1 -0.1 0.1 0.1 -0.1 -0.1 0.1 0.1
  0.25 0.25 0.25 0.25 -0.25 -0.25 -0.25 -0.25
64
-1.1 1.1 1.1 -1.1 -1.1 1.1 1.1 -1.1
  2.9 2.9 3.1 3.1 2.9 2.9 3.1 3.1
  0.25 0.25 0.25 0.25 -0.25 -0.25 -0.25 -0.25
65
-1.1 1.1 1.1 -1.1 -1.1 1.1 1.1 -1.1
  5.9 5.9 6.1 6.1 5.9 5.9 6.1 6.1
  0.25 0.25 0.25 0.25 -0.25 -0.25 -0.25 -0.25

# - Heaters are Copper from Bejan  Air from Bejan also.
rock
  1 0 0 2190. 931. 0.02
-61 0 0 8300. 384. 0.0001

```

```

-62 0 0 8300. 384. 0.0001
-63 0 0 8300. 384. 0.0001
-64 0 0 8300. 384. 0.0001
-65 0 0 8300. 384. 0.0001
-101 0 0 1423. 931. 0.35
-95 0 0 1.1000. 0.999

```

vcon

```

3 26.85 5.4 1.14
4 26.85 1.08 -270. 370. -136. 1.5 5 1.14

```

```

1 0 0 1
-101 0 0 2

```

cond

```

-61 0 0 398. 398. 398.
-62 0 0 398. 398. 398.
-63 0 0 398. 398. 398.
-64 0 0 398. 398. 398.
-65 0 0 398. 398. 398.
-95 0 0 0.03 0.03 0.03

```

perm

```

1 0 0 6.e-20 6.e-20 6.e-20
-101 0 0 1.e-12 1.e-12 1.e-12
-95 0 0 1.e-11 1.e-11 1.e-11

```

#- - - rlp #1 is AIR. #2 is crushed salt #3 is intact salt

rlp

```

1 0. 0. 1.0 1.0 0.0 1.0
3 0.0001 1.0 5.6 1.8 2. 0.005
3 0.0001 1.0 5.6 1.8 2. 0.005

```

```

1 0 0 3
-101 0 0 2
-95 0 0 1
-61 0 0 1
-62 0 0 1
-63 0 0 1
-64 0 0 1
-65 0 0 1

```

Heaters are 1000W(really 500W) = 100Wx5nodes 2e-4MJ/s per node.

divide by two for reflection boundary 1000W = 1.0e-4 MJ/s per node.

hflx

```

-1 0 0 30.00 1.e6
-2 0 0 30.00 1.e6
20403 20404 1 30.00 1.e-4
21653 21654 1 30.00 1.e-4
-61 0 0 -1.0e-4 0.0
-62 0 0 -1.0e-4 0.0
-63 0 0 -1.0e-4 0.0
-64 0 0 -1.0e-4 0.0
-65 0 0 -1.0e-4 0.0
20726 20726 1 -0.5e-4 0.0
20876 20876 1 -0.5e-4 0.0

```

21026 21026 1 -0.5e-4 0.0
 21176 21176 1 -0.5e-4 0.0
 21326 21326 1 -0.5e-4 0.0

ngas
 3
 1 0 0 -30.

1 0 0 0
 20404 20404 1 -0.95751E-01
 21654 21654 1 -0.95751E-01

1 0 0 0

#-----

adif
 0.66

#-----

pres
 1 0 0 6.0 1.000 2
 -61 0 0 0.1 0.000 2
 -62 0 0 0.1 0.000 2
 -63 0 0 0.1 0.000 2
 -64 0 0 0.1 0.000 2
 -65 0 0 0.1 0.000 2
 -95 0 0 0.1 0.0001 2
 -101 0 0 0.1 0.10 2

#----- FLOW

flow
 -1 0 0 6. -30.00 1.e-1
 -2 0 0 6. -30.00 1.e-1
 -3 0 0 6. -30.00 1.e-1

20403 20403 1 0.1 -30. -1.e-5
 # 21653 21653 1 0.1 -30. -1.e-5
 #

#-----

flxz water
 2
 95 101

#-----

time
 1.e-4 730. 5000 10 2012 01 0.0
 20. -1.5 1.0 50 1.0
 50.0 -1.5 1.0 50 2.0
 305. -1.5 1.0 50 1.0
 365. -1.5 1.0 50 1.0

ctrl
 7 1.e-04 08
 1 0 0 1

1.0 3.0 1.0
 10 1.6 1.e-6 2.0
 0 +1

```
iter
1.e-5 1.e-5 1.e-2 -1.e-1 1.0
00 0 0 10 14400.
node
17
  46526 41426 33776 29951 28676 26126 23576 21026 18476 15926 10826 5726 626
  20404 21654 20403 21653
hist
csv
days 1.e7 1.0
water
zflux
mass
flow
global
end
cont
avsx 5000 36.5
pres
temp
liquid
saturation
material
vapor
geo
dens
sat
formatted
endavs
stop
```

Appendix II:

Numerical code to calculate changes in mass in the crushed salt.

```

program satsalt

c Program to calculate the mass of water difference between two *.avsx files
c Adding Parse String to be able to read different formats in avsx files
c NGAS Salt Runs
c days : Liq Pres:Vap Pres (MPa) : Vapor Pressure (MPa) : Water Vap:
c Temperature (deg C) : Saturation : Liquid Density (kg/m**3) : VapDens

implicit none

character*180 filevol1,geo1, zonefile
character*30 file1,file2
character*140 string
real*8 r(100000),z(100000) , y, dumx, dumy, dumz
real*8 density(100000,2)
real*8 pgas(100000,2), sat(100000,2), pwat(100000,2)
real*8 mass1, mass2, days2, days1
real*8 volume(100000)
real*8 rmin, rmax, zmin, zmax, por1, por2,mass1a, mass2a
integer numn1, numn2, i, k , k
integer node, zonen, zonenode(10000)

integer max_entries
parameter(max_entries=20)
integer imsg(max_entries)
integer msg(max_entries)
real*8 xmsg(max_entries)
character*32 cmsg(max_entries)
integer nwds

c-----1-----2-----3-----4-----5-----6-----7

c - - - - - File2 - File1 23 - 22

open(21,file='satdiff.txt')
read(21,*)
read(21,677) file1
read(21,*)
read(21,677) file2
read(21,*)
read(21,669) filevol1
read(21,*)
read(21,669) zonefile
read(21,*)
read(21,*) por1

write(6,*) 'which sca file to process '
read(5,677) file2

```

c - - Hardwire for Salt Simulation 9/25/2012

```

numn1 = 47175

open(22,file=file1)
open(23,file=file2)
open(24,file=filevol1)
open(25,file=zonefile)
open(26,file='satdiff.out')

read(22,679) days1
read(23,679) days2
read(24,*)

do i = 1, numn1
  read(22,671) string
  call parse_string(string,imsg,msg,xmsg,cmsg,nwds)
  pwat(i,1) = xmsg(3)
  pgas(i,1) = xmsg(5)
  sat(i,1) = xmsg(11)
  density(i,1) = xmsg(13)
  if(i.EQ.27277) write(6,*) sat(i,1), density(i,1)
end do

do i = 1, numn1
  read(23,671) string
  call parse_string(string,imsg,msg,xmsg,cmsg,nwds)
  pwat(i,2) = xmsg(3)
  pgas(i,2) = xmsg(5)
  sat(i,2) = xmsg(11)
  density(i,2) = xmsg(13)
  if(i.EQ.27277) write(6,*) sat(i,2), density(i,2)
end do

```

c - - Read in zone information

```

read(25,*)
read(25,*)
read(25,*)
read(25,*) zonen
read(25,*) (zonenode(i), i=1,zonen)

mass1 = 0
mass2 = 0

do i = 1,numn1
  read(24,*) node, volume(i) , dumx, dumy, dumz
end do

do i = 1,zonen
  k = zonenode(i)
  mass1a = density(k,1)*(volume(k)*sat(k,1)*por1)
  mass2a = density(k,2)*(volume(k)*sat(k,2)*por1)
  mass1 = mass1 + mass1a
  mass2 = mass2 + mass2a
  write(26,*) k, mass2a, mass1a, mass2a-mass1a
end do

```

```

end do

write(26,*) 'File1 ', file1, 'days ', days1
write(26,*) 'File2 ', file2, 'days ', days2
write(26,*) 'mass2,mass1,mass file2-file1,(mass2-mass1)/mass1'
write(26,670) mass2,mass1,mass2 - mass1,(mass2-mass1)/mass1

write(6,*) 'File1 ', file1, 'days ', days1
write(6,*) 'File2 ', file2, 'days ', days2
write(6,*) 'mass2,mass1,mass file2-file1,(mass2-mass1)/mass1'
write(6,670) mass2,mass1,mass2 - mass1,(mass2-mass1)/mass1

```

```
c-----1-----2-----3-----4-----5-----6-----7
```

```

550  format(I10,9I11)
668  format(F21.14,3F25.14)
669  format(A140)
670  format(4E16.5)
671  format(a140)
677  format(a30)
679  format('nodes at ',e10.4)

```

```
c-----
```

```
END
```

```
subroutine parse_string(line,msg,xmsg,cmsg,nwds)
```

```
implicit none
```

```
integer max_entries, line_length
parameter(max_entries=20)
character*140 line
integer msg(max_entries)
integer xmsg(max_entries)
real*8 xmsg(max_entries)
character*32 cmsg(max_entries)
integer nwds
logical finished
```

```
integer ndex(max_entries,2),i,begin,entrynum,isinteger,isreal,i2
```

```

line_length = len(line)
entrynum=1
begin=1
do i=1,line_length
  if (((line(i:i).eq.' ').or.(line(i:i).eq.achar(9)))
& .and.(begin.eq.0)) then
    ndex(entrynum,2)=i-1
    begin=1
    entrynum=entrynum+1
  else if ((line(i:i).eq.' ').or.(line(i:i).eq.achar(9))) then
    continue
  else if (begin.eq.1) then
    ndex(entrynum,1)=i

```

```

    begin=0
  else
    continue
  endif
enddo
if (begin.eq.1) entrynum=entrynum-1
nwds=entrynum

do i=1,nwds
  isinteger=1
  isreal=1
  do i2=ndex(i,1),ndex(i,2)
    if (ndex(i,1) .eq. ndex(i,2)) then
c check if just have +, -, e, E, d, or D
      if ( (line(i2:i2).eq.'+') .or. (line(i2:i2).eq.'-') .or.
&        (line(i2:i2).eq.'e') .or. (line(i2:i2).eq.'E') .or.
&        (line(i2:i2).eq.'d') .or. (line(i2:i2).eq.'D') )
&        then
        isreal = 0
        isinteger = 0
        goto 999
      end if
    end if
    if ((line(i2:i2).ne.'+') .and. (line(i2:i2).ne.'-') .and.
&      ((iachar(line(i2:i2)),gt.57) .or.
&      (iachar(line(i2:i2)).lt.48))) isinteger=0
    if ((line(i2:i2).ne.'+') .and. (line(i2:i2).ne.'-') .and.
&      ((iachar(line(i2:i2)),gt.57) .or.
&      (iachar(line(i2:i2)).lt.48)) .and.
&      (line(i2:i2).ne.'e') .and.
&      (line(i2:i2).ne.'E') .and.
&      (line(i2:i2).ne.'d') .and.
&      (line(i2:i2).ne.'D')) isreal=0
  enddo
  if ((isreal.eq.1) .and. (isinteger.eq.0)) then
    msg(i)=2
    read(line(ndex(i,1):ndex(i,2)),*) xmsg(i)
  else if (isinteger.eq.1) then
    msg(i)=1
    read(line(ndex(i,1):ndex(i,2)),*) imsg(i)
  else
    msg(i)=3
    cmsg(i)=line(ndex(i,1):ndex(i,2))
  endif
enddo

999 return
end

```